CVJ
CLUJ VETERINARY JOURNAL

DOI: https://doi.org/10.52331/cvj.v29i1
ISSN: 2066-9399
Cluj Vet J 2023, vol. 29, issue 1
http://clujveterinaryjournal.ro

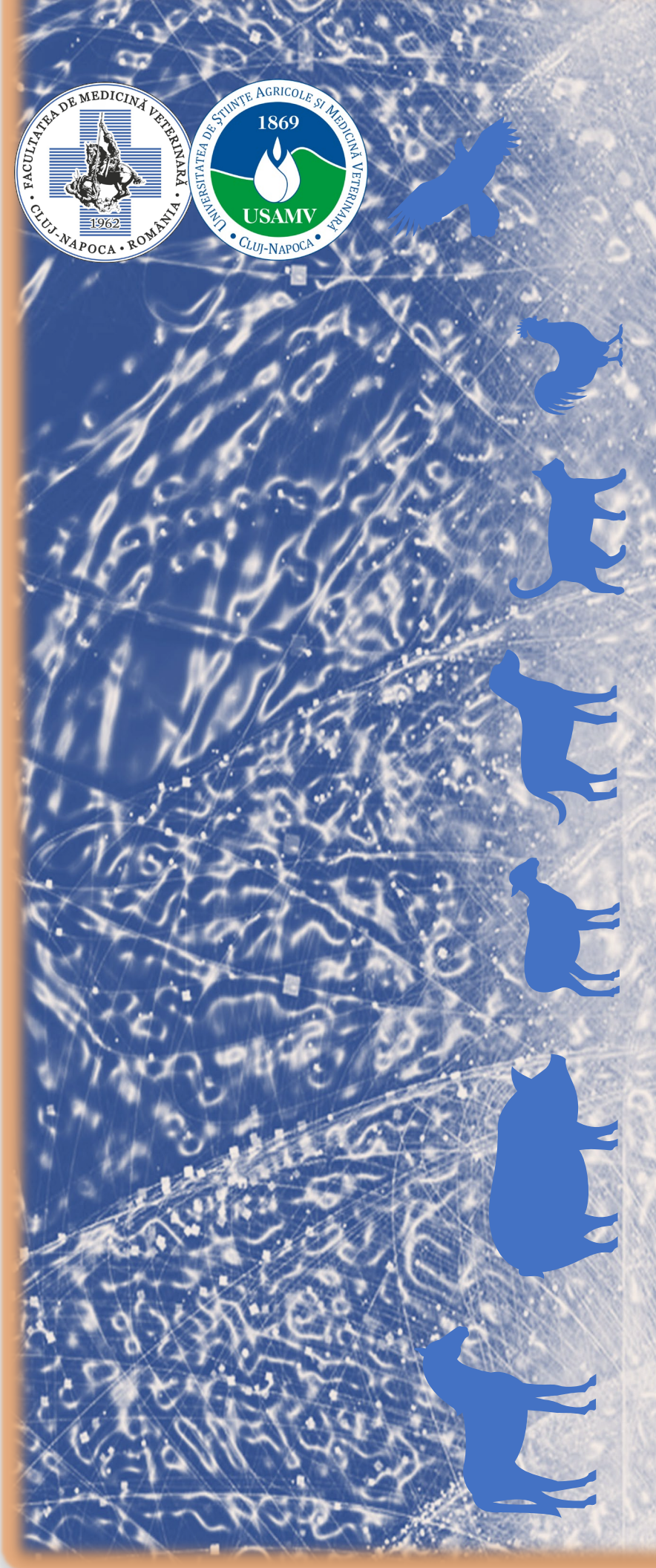

ARTICLES

REVIEW

CVJ CLUJ VETERINARY JOURNAL

Table of contents

CVJ CLUJ VETERINARY JOURNAL

Article

The relationship between Stage B1 Myxomatous Mitral Valve Disease and Cardiac Weight in Dogs: a study on 19 patients

Maria Cerbu [1*] and Ionel Papuc [1]

[1] Department of Comparative Anatomy, Faculty of Veterinary Medicine, University of Agricultural Sciences and Veterinary Medicine, 400372 Cluj-Napoca, Romania; maria.vilcu@usamvcluj.ro, ionel.papuc@usamvcliuj.ro
[2] Affiliation 2; e-mail@e-mail.com
* Correspondence: maria.vilcu@usamvcluj.ro

Abstract: Myxomatous mitral valve disease (MMVD) is a prevalent heart condition in dogs, particularly affecting the mitral valve. Stage B1 of MMVD, as per the American College of Veterinary Internal Medicine (ACVIM) guidelines, encompasses asymptomatic dogs with structural heart disease. This stage is characterized by a range of radiographic and echocardiographic findings without significant cardiac remodeling. Despite its prevalence, the impact of MMVD Stage B1 on cardiac weight remains unclear. In this study, 28 dogs were examined to evaluate if MMVD Stage B1 correlates with abnormal increases in heart weight postmortem. Dogs were clinically examined, underwent echocardiography, and were divided into two groups based on MMVD staging. Heart weight relative to body weight (hW/bW) was assessed. Results revealed that MMVD Stage B1 had minimal impact on heart weight, with hW/bW ratios remaining within normal ranges. Notably, despite differences in breed, sex, and age, hW/bW ratios did not significantly deviate from normal values. This study provides valuable insights into the relationship between MMVD Stage B1 and cardiac weight in dogs, indicating the need for further investigations with larger sample sizes to validate these findings. Understanding cardiac weight alterations in MMVD can aid in refining diagnostic and management approaches for affected dogs.

Keywords: dog; MMVD stage B1; heart weight.

.

Received: 1 April 2024
Accepted: 8 April 2024
Published: 9 April 2024

DOI:10.52331/1d1jh711

1. Introduction

Approximately 10% of dogs presented to primary care veterinary practices are diagnosed with heart disease, with myxomatous mitral valve disease (MMVD) being the most common. In North America, MMVD accounts for approximately 75% of heart pathologies [1]. This pathology is known by various names in literature, including chronic valve disease, degenerative valve disease, endocardiosis, and chronic myxomatous valvular disease [2].

While MMVD primarily affects the mitral valve, it has been reported to affect the mitral valve alone in 62% of dogs, both the mitral and tricuspid valves in 32.5%, and the tricuspid valve alone in 1.3% [3]. The condition is approximately 1.5 times more frequent in males than in females, with higher prevalence observed in smaller dogs (<20 kg). Moreover, the prevalence of MMVD increases markedly with age, particularly in small breed dogs, with up to 85% showing evidence of valve lesions by 13 years of age [1].

Although the precise cause of MMVD remains unknown, it has been established that the disease has an inherited component in some breeds such as Cavalier King

Charles Spaniels [11] and Dachshunds [12]. Additionally, the severity of the disease may have a genetic component in other breeds [1].

The mitral valve leaflets consist of four distinct layers, and when the spongiosa layer thickens, it regains the appearance of mesenchymal tissue, hence the name "myxomatous" [14]. Within the spongiosa layer, myofibroblasts proliferate and form small nodules, which are characteristic of MMVD. Furthermore, endothelial dysfunction promotes thickening of the valve leaflets due to shear stress [2, 13], contrasting with normal atrioventricular valve leaflets, which appear as thin and translucent structures without nodules or thickening at the valve margins [3].

The course of the disease can have four stages of progression: 1) It can start at an older age, progress slowly and never end in heart failure; 2) It progresses slowly and then suddenly, after chordal rupture, progresses rapidly and ends in acute heart failure; 3) It progresses slowly and eventually ends in heart failure; 4) It can progress subclinically and end in sudden death [2].

The American College of Veterinary Internal Medicine (ACVIM) guidelines are commonly used for the clinical classification of dogs with MMVD which describes 4 basic stages of heart disease and heart failure: *Stage A,B,C* and *D* [1].

Stage B identifies dogs with structural heart disease and has 2 subcategories: stage B1 includes asymptomatic dogs that have no radiographic or echocardiographic evidence of cardiac remodeling in response to their MMVD, as well as those in which remodeling changes are present, but not severe enough to meet current clinical trial criteria for treatment initiating [1]; stage B2 refers to asymptomatic dogs that have more advanced mitral valve regurgitation that is hemodynamically severe and long-standing enough to have caused radiographic and echocardiographic findings of left atrial and ventricular enlargement that meet clinical trial criteria used to identify dogs that clearly should benefit from initiating pharmacologic treatment to delay the onset of heart failure [1].

Stage B1 of myxomatous mitral valve disease (MMVD) encompasses a broad spectrum of radiographic and echocardiographic findings. This stage includes dogs with normal left atrial (LA) and left ventricular (LV) dimensions, normal LV systolic function, and normal radiographic vertebral left atrial size (VLAS). However, it also includes patients with echocardiographic or radiographic evidence of left atrial and ventricular enlargement that does not meet specific criteria, such as echocardiographic LA:Ao ratio in the right-sided short axis view in early diastole ≥1.6, left ventricular internal diameter in diastole normalized for body weight (LVIDDN) ≥1.7, and breed-adjusted radiographic vertebral heart score (VHS) >10.5 [1].

In most cases in the B1 ACVIM stage thoracic echocardiography often reveals remodeled, redundant valve tissue extending across the annulus into the left atrium during systole (3). This is accompanied by the presence of a turbulent jet flow at the level of the affected valve, clinicaly expres as a heart murmur with intensity ≥3/6.

Myxomatous degeneration transforms normal thin, translucent leaflets into opaque structures that become thickened in their distal third, progressing to diffuse valve thickening, nodularity, and deformation [3]. A simple classification scheme for grading the severity of gross, myxomatous lesions has been reported and is based upon the degree of leaflet nodularity, thickening, and deformity: Type I lesions represent valve leaflets that contain a few, small, discrete nodules in regions where leaflets contact each other, with areas of opacity in the proximal valve; Type 2 lesions represent leaflets with larger nodules which tend to coalesce at the edges of valve contact, and areas of diffuse opacity may be present; Type 3 lesions comprise larger nodules which have coalesced into irregular, plaque-like deformities, and extend to involve proximal portions of the chordae; Type 4 lesions denote gross distortion and ‘ballooning’ of the valve cusps, and the chordae tendineae are thickened proximally [3].

As part of a complete necropsy examination, a macroscopic and morphometric assessment of the canine heart is required. The first step of this examination involves weighing the heart. Ventricular wall thickness has shown a poor correlation with ventricular mass, so heart weight provides more valid information about possible ventricular hypertrophy, especially in cases of dilation and eccentric hypertrophy [7].

Due to the wide variety of dog somatotypes, accurately assessing cardiac mass requires a ratio of heart weight to total body weight. Few studies have mentioned the heart-to-body weight ratio, with similar results reported: 0.43% to 0.99% [7], 0.6% to 1.1% [5], 0.61% to 0.94% [6], and 0.66% to 1.20% [8]. A wider interval was reported by Ghoshal [9], with a heart-to-bodyweight ratio of 0.5% to 2.2% [5]. Schoning et al. [17]. published similar data for Greyhounds, with results of 1.3 ± 0.2% for females and 1.2 ± 0.2% for males. It is known that the heart-to-body weight ratio is higher in neonates than in adults and varies within species, being higher in more athletic animals (such as horses and dogs) [7].

All the mentioned studies are based on normal macroscopic hearts. In this context, the aim of this study was to evaluate if MMVD stage B1 (ACVIM) can be associated with an abnormal increase in heart weight after postmortem evaluation.

2. Materials and Methods

This research was conducted at the Department of Internal Medicine-Cardiology and Department of Animal Pathology, University of Agricultural Sciences and Veterinary Medicine, Cluj-Napoca, Romania. It involved 28 owner-owned dogs of various breeds, ages (over 1 year old), sexes, and body weights. All dogs underwent a comprehensive clinical examination including assessment of body weight, heart rate, and respiratory rate, followed by a thorough cardiac examination comprising thoracic palpation, auscultation, electrocardiography, and echocardiography. Transthoracic echocardiographic examinations were performed by the same examiner using an Esaote ultrasound (Esaote SpA, Genoa, Italy) equipped with phased-array transducers ranging from 2 to 8 MHz, along with simultaneous single-lead electrocardiography. Dogs were examined from both right and left parasternal positions, obtaining standard echocardiographic 2-dimensional, M-mode, and Doppler images without sedation. For the assessment of ACVIM stage B1, specific echocardiographic criteria were employed. These included the presence of mitral regurgitation (MR) with a mosaic pattern upon color flow Doppler, alongside a normal left atrium (LA) characterized by an echocardiographic LA:Ao ratio <1.6 in the right-sided short-axis view during early diastole. Additionally, normal left ventricular (LV) dimensions and systolic function despite the presence of MR were required. LV measurements, including interventricular septum (IVS), left ventricular internal diameter (LVID), and left ventricular posterior wall (LVPW), were determined in the right parasternal short-axis view using M-mode. Diastolic measurements were taken at the beginning of the QRS complex, while systolic measurements were timed at the shortest distance between the septum and the lateral wall. The leading-edge technique was used for all measurements, as described by Wyatt et al. (1983) [10].

Inclusion criteria: Adult dogs (over 1 year old) with various pathologies, slated for euthanasia, without pre-existing cardiac diseases or with ACVIM stage B1 MMVD as determined by echocardiographic imaging.

Exclusion criteria: Presence of a heart murmur greater than 3/6 on auscultation; morpho-structural thoracic changes hindering quality echocardiographic imaging; administration of any cardio-vascular affecting substance within the previous 14 days; identification of congenital or acquired cardiac anomalies beyond ACVIM stage B1, as detected by 2D echocardiography, M-mode, and Doppler examinations.

Based on the provided criteria, the patients (n=19) were divided into two groups: group 1 (n=13), comprising patients without cardiac disease, and group 2 (n=6), comprising patients with MMVD stage B1 according to ACVIM.

In group 1, there were 7 females and 6 males, with body weights ranging from 7.9 to 65 kg and ages from 2 to 12 years old. The breeds represented were 4 mongrel dogs, 3 German Shepherds, and one each of Tosa Inu, Teckel, Labrador Retriever, Bichon Frise, Dogo Argentino, and Boxer.

In group 2, there were 2 females and 4 males, with body weights ranging from 8 to 43 kg and ages from 10 to 15 years old. Three of them were mongrel dogs, and one each of Golden Retriever, Irish Setter, and West Highland White Terrier.

All dogs from both groups exhibited normal body condition relative to their age and breed. No ECG modifications were observed during a five-minute recording with the patients in lateral recumbency.

The dogs were humanely euthanized (owner consent previusly obtained, in accordance with the national and interntional legislation) , and heart necropsy was performed. The necropsy examination was conducted with the dogs in lateral decubitus on the left side, with the abdomen dorsal. The entire cardiorespiratory system was dissected from the level of the tongue to the diaphragm. Initial inspection of the heart was done together with the lungs before separation. The pericardium was removed for proper macroscopic examination. Residual blood clots and large vessels were eliminated, and the heart was weighed using the same scale, with the weight noted in grams.

3. Results

The results of the study are presented in Tables 1 and 2. The relationship between heart weight and body weight (hW/bW) was assessed individually, indicating that the heart weight represented 0.44% to 1.11% of the animal's body weight for group 1 and 0.51% to 0.93% for group 2.

Table 1. Results obtained from group 1 (free of cardiac pathologies)

No.	Breed	Age (years)	Sex	Weight (kg)	Cardiac murmur	Cardiac pathology	hW/bW ratio
1	Tosa Innu	8	F	26	No	No	0,79
2	Teckel	4	F	9,8	No	No	0,85
3	Mongrel dog	2	F	26,3	No	No	0,66
4	Mongrel dog	10	M	30,7	No	No	0,86
5	Labrador Retriever	7	F	36	No	No	0,57
6	German Shepard	8	M	38,7	No	No	0,77
7	Bichon Frise	5	M	7,9	No	No	0,94
8	German Shepard	12	F	18,1	No	No	1,03
9	Mongrel dog	3	M	40	No	No	0,68
10	Dogo Argentino	2	M	40	No	No	0,7

11	German Shepard	6	F	23,6	No	No	1,11
12	Mongrel dog	6	M	65	No	No	0,44
13	Boxer	5	F	27	No	No	0,74

bW= body weight; hW= heart weight.

Table 2. Results obtained from group 2 (with MMVD stage B1).

No.	Breed	Age (years)	Sex	Weight (kg)	Cardiac murmur	Cardiac pathology	hW/bW ratio
1	Mongrel dog	10	F	8	Yes	Yes	0,78
2	Mongrel dog	15	M	30	Yes	Yes	0,55
3	Mongrel dog	13	F	21,4	Yes	Yes	0,85
4	Golden Retriever	10	M	23,2	No	Yes	0,93
5	Irish Setter	13	M	43	No	Yes	0,51
6	West Highland White Terrier	12	M	9,8	No	Yes	0,88

4. Discussion

Cardiac diseases often manifest through changes in the size and weight of specific heart components, with the degree of change typically proportional to the severity of the disease, as seen in hypertrophic and dilated cardiomyopathies [5, 18].

Stage B1 (ACVIM) represents perhaps the most common yet underdiagnosed form of MMVD, characterized by the absence of clinical signs. In this stage, the heart murmur may be of low intensity and even be missed by the examiner during cardiac auscultation. Additionally, ECG and thoracic radiographs may show no significant changes, further complicating diagnosis. Consequently, Stage B1 represents a gray area in MMVD, where pathology exists but without clinical signs and without the need for treatment at this stage.

In group 2, all patients showed no clinical signs attributable to cardiac pathology, had normal ECG readings, but exhibited an audible heart murmur ranging in intensity from 1/6 to 3/6.

The likelihood of ACVIM stage B1 of MMVD affecting total cardiac weight is diminished, given that the valvular apparatus is the primary element impacted. This fact is corroborated by the results obtained in this study. However, significant weight variations may occur from ACVIM stage B2 onwards, indicating substantial cardiac remodeling as identified by echocardiography. Exploring the correlation between left ventricular mass and total body weight across different ACVIM MMVD stages could be a promising avenue for future research. Such a study could reveal more notable differences in values due to the nature and progression of the pathology, which affects the left ventricle in 62% of cases [3].

An overview of the age distribution among the patients involved in the study reveals a higher average age for the dogs included in group 2, supporting the hypothesis of a higher incidence of cardiac pathology in geriatric patients [1]. MMVD is widely recognized as a disease of the aging heart, as extensively described by

Connell et al. [4]. Despite two patients being classified as large breed dogs, specifically a Golden Retriever and an Irish Setter, it can be inferred that the remainder of patients in group 2 are predominantly medium to small-sized dogs, which is also a risk factor and predictor for cardiac pathology. It's commonly observed that small dogs tend to live longer on average than large dogs, potentially contributing to the development of MMVD in smaller breeds [3].

The hW/bW ratio results in both groups were within normal ranges, with only 4 values falling below the minimum range, set at 0.6%. However, when compared to Ghoshal's findings (9), which reported a wider range of 0.5% to 2.2%, only one value fell below the lower limit. This value, at 0.44%, was observed in a noncardiac mongrel dog (male) weighing 65 kg. Values below 0.6% were observed in both groups. Among the cardiac patients, an Irish Setter exhibited a ratio of 0.51%, and a 30 kg male mongrel dog had a ratio of 0.55%. The noncardiac patient, a female Labrador Retriever weighing 36 kg, had a ratio of 0.57%.

Only two values exceeded 1%, both found in female German Shepherds without cardiac diseases. In group 2, no value reached 1%, and none of the patients reached the maximum value of 2.2% reported by Ghoshal [9]. Consistent with other studies, neither breed, sex, nor age of adult dogs influenced the hW/bW ratio [5, 6, 17].

An important factor that should not be overlooked and can significantly influence the hW/bW ratio investigated in this study is the patient's body condition score (BCS). BCS is a numeric evaluation system commonly used to assess body fat accumulation [15], with the 9-point scale being most frequently employed in dogs [16]. Utilizing this scale helps reduce subjectivity in the assessment. Excessive body fat accumulation leading to overweight or obesity in dogs may result in a low or normal hW/bW ratio. Conversely, various pathologies can induce cachexia in a patient, potentially leading to a falsely higher ratio than the normal range. Therefore, evaluating BCS before or during necropsy examination is becoming increasingly essential. Although the dogs involved in this study were neither obese nor emaciated, a formal BCS assessment was not performed.

Additionally, previous studies [5-8, 17]. considered dogs to have normal weight based on subjective assessments. Overweight dogs could provide a valid explanation for the lower results observed in this study. For instance, the values of 0.44% and 0.51% were obtained from dogs with the highest weights, 65 kg and 43 kg, respectively. However, the value of 0.44% may still be considered normal according to references provided by some authors [7].

The novelty of this study lies in its comprehensive approach, which involves both pre- and post-necropsy examinations of the heart, a methodology not previously employed in existing studies [5-9]. Previous studies typically examined dogs without the clinical examination being complemented by ultrasound, and the heart was considered normal based solely on macroscopic examination during necropsy.

Estimating cardiac hypertrophy at necropsy is typically attempted through various methods, including gross observation of cardiac structure, measurements of ventricular wall thickness, and weighing of the heart in relation to body weight [5]. However, the variations in heart weight depending on cardiac pathology remain largely unknown, as there are no published studies of this nature. Therefore, this study fills an important gap in the literature by providing a more detailed and nuanced understanding of cardiac pathology and its impact on heart weight.

5. Conclusions

The ACVIM stage B1 of MMVD has a minor effect on heart weight, keeping the hW/bW ratio within the normal range. Further research is needed due to the limited patient pool. These findings provide a foundation for calculating this ratio across different ACVIM stages. Results for noncardiac patients align with past studies.

Author Contributions: Conceptualization, M.C. and I.P.; methodology, investigation, M.C. and I.P.; writing—original draft preparation, MC.; writing—review and editing, I.P.; supervision, I.P.; All authors have read and agreed to the published version of the manuscript.

Institutional Review Board Statement: Ethical review and approval were waived for this study due to preexisting conditions in the dogs, which included recommended euthanasia based on previously obtained consent from the owners.

Data Availability Statement: For further information, please contact the corresponding author via email.

Conflicts of Interest: The authors declare no conflict of interest.

References

1. Keene, B. W., Atkins, C. E., Bonagura, J. D., Fox, P. R., Häggström, J., Fuentes, V. L., ... & Uechi, M. (2019). ACVIM consensus guidelines for the diagnosis and treatment of myxomatous mitral valve disease in dogs. *Journal of veterinary internal medicine*, 33(3), 1127-1140.
2. Petrič, A. D. (2015). Myxomatous mitral valve disease in dogs-An update and perspectives. *Macedonian veterinary review*, 38(1), 13-20.
3. Fox, P. R. (2012). Pathology of myxomatous mitral valve disease in the dog. *Journal of Veterinary Cardiology*, *14*(1), 103-126.
4. Parker, H. G., & Kilroy-Glynn, P. (2012). Myxomatous mitral valve disease in dogs: does size matter?. *Journal of veterinary cardiology*, *14*(1), 19-29.
5. Queiroz, L. L., Moura, L. R., & Moura, V. M. B. D. (2018). Morphometric assessment of canine heart without macroscopically visible changes caused by cardiac disease. *Ciência Animal Brasileira*, *19*, e43748.
6. Bienvenu, J. G., & Drolet, R. (1991). A quantitative study of cardiac ventricular mass in dogs. *Canadian Journal of Veterinary Research*, 55(4), 305.
7. Robinson, W.F., Robinson, N.A.: Cardiovascular System. In Jubb, Kennedy & Palmer's *Pathology of Domestic Animals - volume 3. 6th edition*. Edited by Maxie MG. London: Elsevier Saunders. 2015;1–101.
8. Carvalho, L. M. M., Andrade, F. H. E., Alves, F. R., Guerra, P. C., & Sousa, A. L. (2002). Morfometria cardíaca externa em cães adultos. *Pesquisa em Foco*, *10*, 1-2.
9. Ghoshal, N.G.: Coração e artérias do carnívoro. In *Anatomia dos Animais Domésticos. 5th edition*. Edited by Getty R, Sisson S, Grossman JD. Rio de Janeiro: Guanabara Koogan. 1986;1497–1549
10. Wyatt, H. L., Haendchen, R. V., Meerbaum, S., & Corday, E. (1983). Assessment of quantitative methods for 2-dimensional echocardiography. *The American Journal of Cardiology*, *52*(3), 396-401.
11. Madsen, M. B., Olsen, L. H., Häggström, J., Höglund, K., Ljungvall, I., Falk, T., ... & Fredholm, M. (2011). Identification of 2 loci associated with development of myxomatous mitral valve disease in Cavalier King Charles Spaniels. *Journal of Heredity*, *102*(Suppl_1), S62-S67.
12. Olsen, L. H., Fredholm, M., & Pedersen, H. D. (1999). Epidemiology and inheritance of mitral valve prolapse in Dachshunds. *Journal of veterinary internal medicine*, *13*(5), 448-456.
13. Pedersen, H.D. (2000). Mitral valve prolapse in the dog. Pathogenesis, pathophysiology and comparative aspects or early myxomatous mitral valve disease. PhD thesis, Copenhagen
14. Kittleson, M.D. (2005). Myxomatous mitral valve disease. In: Kittleson, M.D. and Kienle R.D. *Small Animal Cardiovascular Medicine*, Mosby
15. Chun, J. L., Bang, H. T., Ji, S. Y., Jeong, J. Y., Kim, M., Kim, B., ... & Kim, K. H. (2019). A simple method to evaluate body condition score to maintain the optimal body weight in dogs. *Journal of animal science and technology*, 61(6), 366.
16. Laflamme, D. R. P. C., Developmental and validation of a body condition score system for dogs. (1997): 10-15.
17. Schoning, P., Erickson, H., & Milliken, G. A. (1995). Body weight, heart weight, and heart-to-body weight ratio in greyhounds. *American journal of veterinary research*, *56*(4), 420-422.
18. Werner, P. R., Bolson, J., & Battisti, M. K. B. (2001). Morfometria cardíaca para o diagnóstico de cardiopatias em cães. *Arq. ciênc. vet. zool. UNIPAR*, 181-188.

CVJ CLUJ VETERINARY JOURNAL

Article

Distribution and functional significance of muscle islands in the tunica media of the aorta in the goat (*Capra hircus*)

Cosmin-Rareș Creț[1], Melania Ioana Crișan[1,*], Radu Constantinescu[2], Călin Lațiu[2], Mircea Cipou[3], Cristian Olimpiu Martonoș[1,4] and Aurel Damian[1]

1. Faculty of Veterinary Medicine, University of Agricultural Sciences and Veterinary Medicine Cluj-Napoca, 400372 Cluj-Napoca, Romania
2. Faculty of Animal Science and Biotechnologies, University of Agricultural Sciences and Veterinary Medicine Cluj-Napoca, , 400372, Romania
3. Assisi Veterinary Clinic, Swords, Co. Dublin, Ireland
4. School of Veterinary Medicine, Ross University, Basseterre P.O. Box 334, Saint Kitts and Nevis

* Correspondence: melania.crisan@gmail.com;

Abstract: The presence of muscle islands in the tunica media of elastic arteries has been reported in both large and small ruminants. According to some authors, these islands can have a certain influence on the physical-mechanical properties and the pattern of diseases in the aortic wall. The aim of the current study was to highlight the muscle islands and their distribution throughout the aortic segments in the goat and to understand the reason why they are present only in certain species of animals, including the goat. Gross anatomical dissection of the aorta was performed and samples from the following segments were harvested for histological investigations: ascending aorta, aortic arch, descending thoracic aorta and descending abdominal aorta. The muscle islands in the wall of the aortic segments are formed by smooth muscle cells interconnected with connective tissue and are preferentially vascularized by vasa vasorum and innervated by nervi vasorum. The aorta in the goat presents polymorphic muscle islands, arranged in the outer two thirds of the tunica media in the ascending aorta, the outer half at the level of the aortic arch and the descending thoracic aorta, but they are absent in the descending abdominal aorta. Their presence completes the windkessel function of the aortic wall, thus constituting an additional pump necessary to propel the blood towards the abdominal viscera, which in goats, in addition to those present in monogastrics, also contain three large and very active organs, namely the rumen, the reticulum and the omasum.

Keywords: goat, aorta, tunica media, muscle islands

Received: 13 December 2023
Accepted: 14 February 2024
Published: 9 April 2024

DOI:10.52331/z3nc1197

1. Introduction

During ventricular systole, blood is forced into the aorta in the form of intermittent jets, so it exerts a certain pressure on the vascular walls. Due to this pressure, the elastic structures in the wall of the arteries expand and store part of the pressure exerted on them, causing the dilation of the arterial lumen, to take over the surplus blood that arrives here during the ventricular systole. During diastole, the elastic fibers passively contract and return to their original size, causing excess blood to propel to the next segments. In this way, the elastic fibers produce what is called the windkessel effect during ventricular systole and diastole [1]. The muscle cells existing between the elastic lamellae complement the action of the elastic fibers through active contraction, so that through the action of the elastic

and muscular components, blood flow becomes continuous in the following vessels [2].

In elastic arteries, the thickest tunic is the media containing the concentric elastic lamellae, between which there are circularly arranged smooth muscle fibers, collagen fibers, and reticular fibers [3]. These components have a particular arrangement among the elastic lamellae, which ensures their participation in completing the windkessel mechanism. In lower pressure arteries such as the abdominal descending aorta, the windkessel mechanism is complemented by a prominent internal elastic limiter [4].

In some species of mammals, the muscle component in the middle of the elastic arteries appears significantly better represented and with a particular disposition. Thus, [5] found that in the goat, the tunica media of the ascending aorta, the aortic arch and the descending thoracic aorta, present two areas: the luminal elastic area, which has a structure comparable to that of elastic arteries from other species, and the adventitial musculo-elastic area, in which elastic lamellae are zonally interrupted by polymorphic muscle islands. The presence of muscle islands in the tunica media of elastic arteries has been reported in both large and small ruminants [6-9]. According to some authors, these islands can have a certain influence on the physical-mechanical properties and the pattern of diseases in the aortic wall [9]. The aim of the current study was to highlight the muscle islands and their distribution throughout the aortic segments in the goat and to understand the reason why they are present only in certain species of animals, including the goat.

2. Materials and Methods

The biological material used in this study was represented by 5 adult goats, of common breed, slaughtered for consumption in a CE approved slaughterhouse. The study was conducted according to the guidelines of the Declaration of Helsinki, and approved by the Bioethics Committee of the University of Agricultural Sciences and Veterinary Medicine Cluj-Napoca, nr. 403 from 29.09.2023. The AVMA guidelines set criteria for euthanasia were followed, and the procedure was in line with the recommendations of the permanent OIE (World Organisation for Animal Health) Animal Welfare Working Group for Humane slaughter of animals.

Gross anatomical dissection of the aorta was performed and samples from the following segments were harvested for histological investigations: ascending aorta, aortic arch, descending thoracic aorta and descending abdominal aorta. The samples were fixed in 10% formalin solution for 7 days, then dehydrated in three successive baths of ethyl alcohol (70%, 96%, and absolute), clarified with three baths of 1-Butanol and embedded in paraffin. Sections with a thickness of 5 μm were made, which were stained by the Trichrome Goldner method. The obtained preparations were examined under an Olympus BX41 microscope, equipped with a digital camera for capturing images, model Olympus E-330.

3. Results

The first segment of the arterial system at the exit from the heart is the ascending aorta, which in the goat has a very peculiar wall structure, differing in some respects from that of most mammals. These particularities are found in the media, while the intima and adventitia are comparable to the existing situation in other mammals. The particularity consists in the fact that the ratio between the elastic and the muscular component is different here and the disposition of the muscular component has some particularities. In the media of the ascending aorta of the goat, two areas can be distinguished, an internal one that occupies approximately 40% of the wall thickness that has the appearance found in the elastic arteries of other mammalian species, and an external one that occupies approximately 60% of the wall thickness in which the muscular component it is much better represented compared to the intima. Here the muscle component forms islands arranged

at a certain distance from each other, without respecting a rigorous distribution. Islets are polymorphic in both shape and size and even muscle cell orientation (Fig. 1).

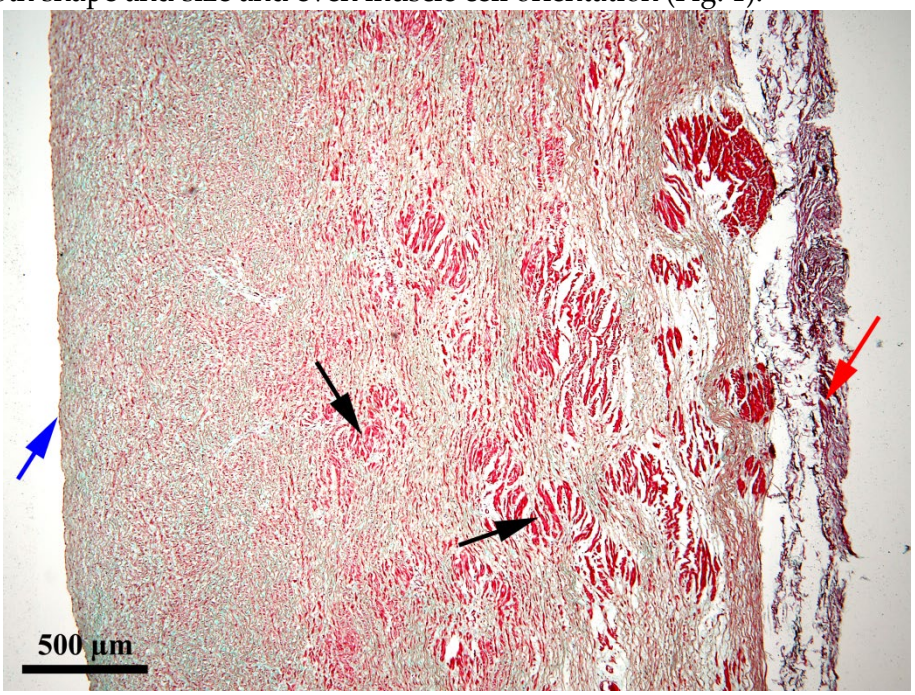

Figure 1. Ascending aorta of the domestic goat (ob. 4X)

Black arrow: muscle islands in tunica media; red arrow – tunica adventitia; blue arrow - tunica intima

The situation is largely the same in the middle of the aortic arch, both in terms of the presence, distribution, shape, density or appearance of the muscle islands in the tunica media. (Fig. 2).

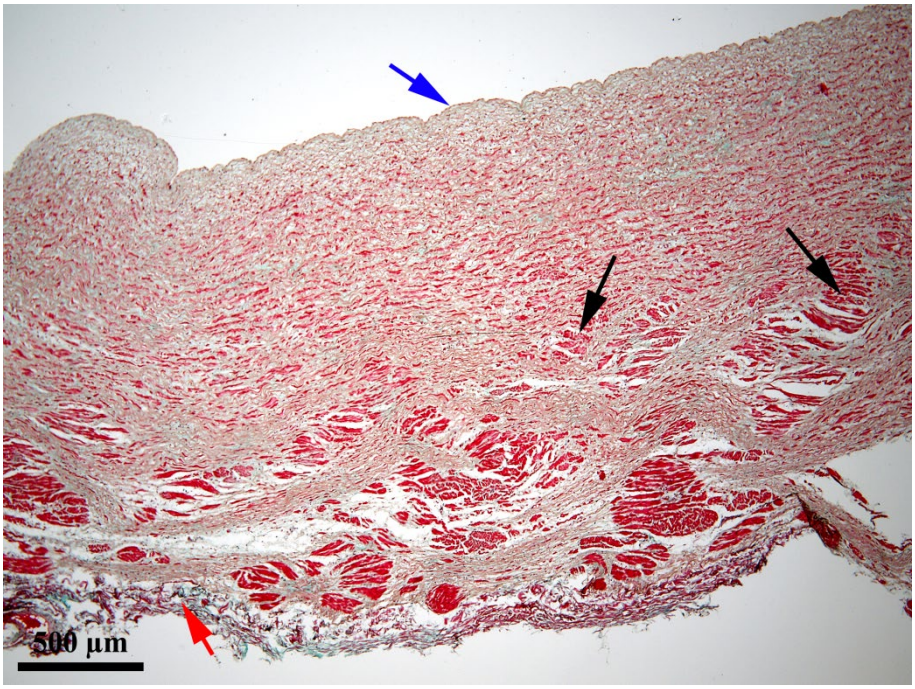

Fig. 2 Aortic arch (ob 4X)

Black arrow: muscle islands in tunica media; red arrow – tunica adventitia; blue arrow - tunica intima

In the descending thoracic aorta, the situation is similar to that existing at the level of the aortic arch, which is otherwise continued by this arterial segment. Muscle islands are numerous, with the most and larger islands being found in the outer third of the media versus the middle where the islands are somewhat scarce and the muscle cells less dense (Fig. 3).

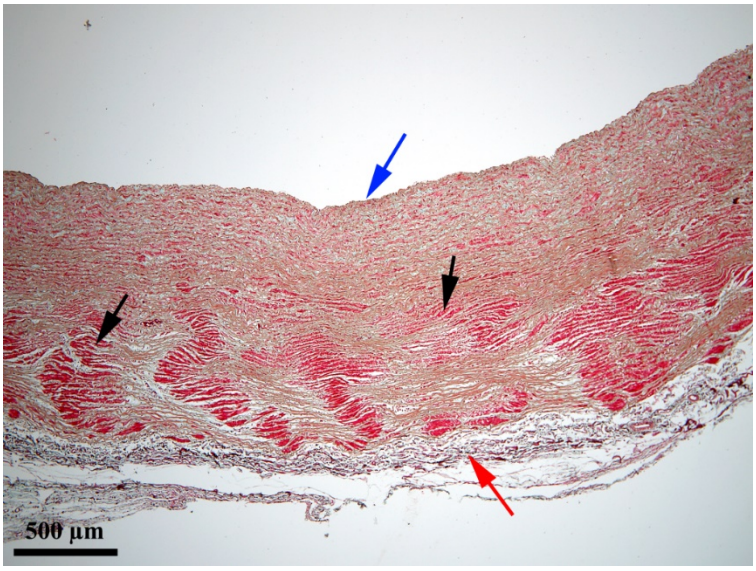

Fig. 3 Descending aorta – thoracic segment 221 (ob 4X)

Black arrow: muscle islands in tunica media; red arrow – tunica adventitia; blue arrow - tunica intima

The situation changes radically at the level of the descending abdominal aorta where muscle islands are no longer found as in the previous segments, but the general appearance is that of a typical elastic artery in which the main component is the elastic one represented by relatively rigorously arranged wavy elastic lamellae and between them cells muscle and collagen fibers. It should be noted that the adventitia of the descending abdominal aorta is thicker than that at the level of the ascending aorta, the aortic arch and the descending thoracic aorta (Fig. 4).

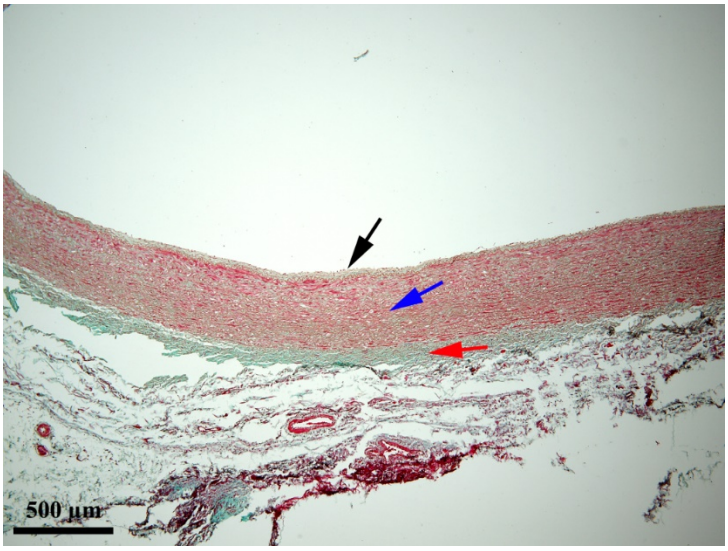

Fig. 4 Descending aorta – abdominal segment 345 (ob. 4)

Black arrow: tunica intima; blue arrow - tunica intima; red arrow – tunica adventitia

4. Discussion

In our study, we found the presence of polymorphic muscle islands in the middle of the ascending aorta, aortic arch, and descending thoracic aorta, but not in the descending abdominal aorta. These muscular islands zonally interrupt the concentric elastic lamellae characteristic of elastic arteries. In terms of number and location, the muscle islands were the most and largest in the ascending aorta, for their number and size to decrease progressively so that at the level of the abdominal aorta they disappeared completely. As an extension they are present in the outer 2/3 of the media in the ascending aorta and in the outer half in the case of the aortic arch and the descending thoracic aorta. Muscle islands present in the external half of the media were also identified by [10] in ascending aorta, aortic arch and goat thoracic aorta up to T9. From T10 and T11, the islands visibly decreased in both size and arrangement, being present here only in the outer third of the media. At the level of the abdominal descending aorta, the muscle islands were no longer found. The presence of muscle islands only in the proximal segments of the aorta suggests that they are related to the blood pressure aspects of each segment. At least two functions have been attributed to these muscle islands: strengthening the aortic wall and supplementing the windkessel function [8,9].

A gradual decrease was also noted in the case of elastic lamellae, an aspect that seems to be directly related to the stress given by blood pressure [11,12]. Blood propelled from the heart exerts the greatest tension on the ascending aorta, then the aortic arch and the proximal portion of the thoracic descending aorta. The structure of the walls of these aortic segments provides an elastic recoil that causes blood flow to become continuous and under significantly reduced pressure in the abdominal descending aorta [11]. In this context, the descending abdominal aorta has a lower number of elastic lamellae than the cranial segments, an aspect that has also been reported in humans [13]. Due to this similarity, we believe that among the goat aortic segments, the only one that lends itself as a model for studying aortic diseases in humans is the abdominal descending aorta. Being adapted to lower blood pressure than the cranial aortic segments, the goat abdominal descending aorta is structurally weaker than the thoracic aorta. This aspect appears to make it more vulnerable (prone) to atherosclerosis and aneurysm formation compared to the thoracic lineage [10, 14]. But there are also conditions such as penetrating atherosclerotic ulcers, which occur more frequently in the thoracic than in the abdominal lineage [15,16].

The muscle islands in the wall of the aortic segments are formed by smooth muscle cells interconnected with connective tissue and are preferentially vascularized by vasa vasorum and innervated by nervi vasorum. During ventricular systole, the blood is forced as a jet into the aorta, the elastic lamellae stretch and due to the fact that they are interconnected with the muscle cells, they pull the muscle islands, which also stretch to some extent. During diastole, by the rebound of the elastic lamellae, the excess blood is pushed to the next segments, and the muscle cells contract and complete the action of the elastic lamellae. These muscle islands thus represent an auxiliary pump that helps propel the blood by amplifying the elastic recoil during diastole but also ensures the increase of the mechanical resistance of the aortic wall [9]. Some authors claim that the muscle islands are probably involved in the regulation of blood flow to certain anatomical regions, more requested in a certain period. An argument in support of this statement is the fact that a similar arrangement allows for drastic circulatory changes in the posterior part of the bird's body during flight [17]. Another example is the regulation of blood flow for the brachiocephalic trunk and

common carotids in the giraffe [18]. These examples suggest the continuous adaptation of animals regarding feeding and locomotion with and against gravity [1]. These examples suggest that muscle islands constitute an auxiliary pump in vessels that conduct blood in a cranial direction, while the aortic segments taken in our study conduct blood in a caudal direction. The presence of muscle islands in the wall of very well represented goat aortic segments suggests the need for an auxiliary pump to propel blood caudally. In other words, the goat needs a larger amount of blood sent to the abdominal viscera than other species of comparable size. The explanation is the fact that the goat's digestive system contains three organs in addition to monogastric animals, namely the rumen, the reticulum and the omasum. These organs, in addition to being large, are also very actively involved in the complex digestion process characteristic of ruminants. The existence of these gastric compartments makes the need for blood sent through the aorta greater in a polygastric animal than in a monogastric of comparable size. This would explain why, in the goat, the aortic media requires this additional blood propulsion pump to provide the right amount of blood and pressure to supply the viscera.

5. Conclusions

The aorta in the goat presents polymorphic muscle islands, arranged in the outer two thirds of the tunica media in the ascending aorta, the outer half at the level of the aortic arch and the descending thoracic aorta, but they are absent in the descending abdominal aorta. Their presence completes the windkessel function of the aortic wall, thus constituting an additional pump necessary to propel the blood towards the abdominal viscera, which in goats, in addition to those present in monogastrics, also contain three large and very active organs, namely the rumen, the reticulum and the omasum.

Author Contributions:
Conceptualization: Rareș Cosmin Crețț, Melania I. Crișan, and Aurel Damian; methodology: Cristian Olimpiu Martonos, Mircea Cipou and Aurel Damian; software : Radu Constantinescu and Călin Lațiu; writing—original draft preparation: Melania Ioana Crișan; writing—review and editing: Melania I. Crișan, supervision - Aurel Damian. All authors have read and agreed to the published version of the manuscript.

Funding: This research received no external funding

Institutional Review Board Statement: The study was conducted according to the guidelines of the Declaration of Helsinki, and approved by the Bioethics Committee of the University of Agricultural Sciences and Veterinary Medicine Cluj-Napoca, nr. 403 from 29.09.2023.

Acknowledgments: In this section, you can acknowledge any support given which is not covered by the author contribution or funding sections. This may include administrative and technical support, or donations in kind (e.g., materials used for experiments).

Conflicts of Interest: The authors declare no conflict of interest.

References

1. Shakuntala Rao N., Sujatha K., Meera K., Krishna Rao H.R. A comparative study on the structure and functions of aorta in man and ruminant animals. 2016,., Int J Anat Res. Volume 4(4):3194-98. DOI:10.16965/ijar.2016.437
2. Gal A.F., Miclăuș V., *Histologie specială și Embriologie generală.* Publisher: Editura AcademicPres, Cluj-Napoca, Romania, 2020. pp: 6-12, e-ISBN: 978-973-744-837-8.
3. Sharanagouda, Ashok P, Dilipkumar D,et al. Comparative histomorphology and histochemistry of thoracic aorta in deccani sheep and bidri goat. MOJ Anat Physiol. 2016. Volume 2(3):55–59. DOI: 10.15406/mojap.2016.02.00044

4. Silver FH, Snowhill PB, Foran DJ. Mechanical behavior of vessel wall: a comparative study of aorta, vena cava, and carotid artery. Ann Biomed Eng. 2003 Jul-Aug. Volume 31(7):793-803. doi: 10.1114/1.1581287. PMID: 12971612.
5. Ogeng'o JA, Malek AAK, Kiama SG, Olabu BO., 2009, Muscle "islands" in the tunica media of the goat thoracic aorta. J Morphol Sci; 26: 171–175.
6. Knieriem HJ. Electron-microscopic study of bovine arteriosclerotic lesions. Am J Pathol. 1967 Jun. Volume 50(6):1035-65. PMID: 6067318; PMCID: PMC1965354.
7. Fukuda Y, Ferrans VJ, Crystal RG. Development of elastic fibers of nuchal ligament, aorta, and lung of fetal and post-natal sheep: an ultrastructural and electron microscopic immunohistochemical study. Am J Anat. 1984 Aug; Volume 170(4):597-629. doi: 10.1002/aja.1001700407. PMID: 6475819.
8. Malek AKA, Ogeng'o J., 2007, Regional differences in the tunica media of the aorta of the goat (cabra ibex). Proceedings of the Winter Meeting of Anatomical Society of Britain and Ireland, Oxford Jan 3 – 5, 2007 Pg 9.
9. Ogeng'o, JA., Malek, AAK., Kiama, SG. and Olabu, BO. Muscle "islands" in the tunica media of the goat thoracic aorta Braz. J. Morphol. Sci. 2009. Volume 26 (3-4): 171-175.
10. Ogeng'o JA, Malek AK, Kiama SG. Regional differences in aorta of goat (capra hircus). Folia Morphol (Warsz). 2010 Nov;69(4):253-7. PMID: 21120813.
11. Orsi AM, Stefanini MA, Crocci AJ, Simões K, Ribeiro AA. Some segmental features on the structure of the aortic wall of the dog. Anat Histol Embryol. 2004 Jun. Volume 33(3):131-4. doi: 10.1111/j.1439-0264.2004.00410.x. PMID: 15144278.
12. Sokolis DP, Boudoulas H, Kavantzas NG, Kostomitsopoulos N, Agapitos EV, Karayannacos PE. A morphometric study of the structural characteristics of the aorta in pigs using an image analysis method. Anat Histol Embryol. 2002 Feb. Volume 31(1):21-30. doi: 10.1046/j.1439-0264.2002.00356.x. PMID: 11841354.
13. Wolinsky H, Glagov S. Comparison of abdominal and thoracic aortic medial structure in mammals. Deviation of man from the usual pattern. Circ Res. 1969 Dec. Volume 25(6):677-86. doi: 10.1161/01.res.25.6.677. PMID: 5364644.
14. Hoffman GS. Determinants of vessel targeting in vasculitis. Ann N Y Acad Sci. 2005 Jun. Volume 1051:332-9. doi: 10.1196/annals.1361.075. PMID: 16126975.
15. Chiche L, Lesèche G. Les ulcères athéromateux pénétrants de l'aorte [Penetrating atheromatous ulcers of the aorta]. Presse Med. 2000 Mar 25. Volume 29(11):611-8. French. PMID: 10776419.
16. Cho KR, Stanson AW, Potter DD, Cherry KJ, Schaff HV, Sundt TM 3rd. Penetrating atherosclerotic ulcer of the descending thoracic aorta and arch. J Thorac Cardiovasc Surg. 2004 May; Volume 127(5):1393-9; discussion 1399-1401. doi: 10.1016/j.jtcvs.2003.11.050. PMID: 15115998.
17. Berry, CL., Germain, J. and Lovell, P. Comparison of aortic lamellar unit structure in birds and mammals. Atherosclerosis. 1974. Volume 19 (1): 47-59.
18. Kimani, JK. and Opole, IO. The structural organization and adrenergic innervation of the carotid arterial system of the Giraffe (*Giraffa Camelopardalis*). The Anatomical Record. 1991. Volume 230 (3): 360-377.

CVJ CLUJ VETERINARY JOURNAL

Research Article

Correlating Eosin Fluorescence Patterns and Basophilic Alterations in a DEN-Induced HCC Murine Model Through Confocal Microscopy

Romelia Pop [1]*, Dragoș Hodor[1], Cornel Cătoi[1], Teodora Mocan[2,3], Lucian Mocan[2,4] and Alexandru-Flaviu Tăbăran[1]

[1] Department of Pathology, Faculty of Veterinary Medicine, University of Agricultural Sciences and Veterinary Medicine of Cluj-Napoca, Calea Manașstur, 400372 Cluj-Napoca, Romania; romelia.pop@usamvcluj.ro; dragos.hodor@usamvcluj.ro; cornel.catoi@usamvcluj.ro; alexandru.tabaran@usamvcluj.ro;
[2] Nanomedicine Department, Regional Institute of Gastroenterology and Hepatology "Octavian Fodor";
[3] Department of Physiology, University of Medicine and Pharmacy, "Iuliu Hatieganu"; teodora.mocan@umfcluj.ro
[4] 3-rd Surgery Clinic, University of Medicine and Pharmacy, 400162 Cluj-Napoca, Romania; lucian.mocan@umfcluj.ro
*Correspondence: romelia.pop@usamvcluj.ro; Tel: +40744263975

Abstract: Hepatocellular carcinoma is a major global health concern and a leading cause of cancer-related mortality. This study employed chemically induced murine models to simulate human hepatocellular carcinoma, utilizing 28 albino Swiss mice with the administration of a single dose of the complete carcinogen diethylnitrosamine (DEN) at 100mg/kg, followed by serial euthanasia. The focus was on understanding early hepatocellular alterations and distinguishing precursor changes from incidental changes. The assessment of hepatocellular alteration foci relied on hematoxylin and eosin (H&E) staining. However, the research introduced a novel approach by exploiting the fluorescence properties of eosin, a component of the H&E stain. This approach was applied to investigate basophilic alteration foci indicating alterations in cellular composition exhibiting notably heightened RNA staining. To achieve this, confocal laser scanning microscopy was employed, correlating changes in fluorescence intensity with tinctorial alterations. The histological examination revealed that basophilic foci displayed unique nodular lesions with intense basophilic cytoplasm. Nuclear alterations, including hyperchromasia and basophilia, contributed to understanding cellular and nuclear changes in these foci. Statistical analysis highlighted a discernible reduction in eosin fluorescence intensity within basophilic foci compared to normal hepatic tissue.

Keywords: hepatocellular carcinoma; animal model; basophilic foci; histology, eosin, confocal microscopy

1. Introduction

Received: 14 December 2023
Accepted: 15 March 2024
Published: 9 April 2024

DOI:10.52331/nqpej009

Hepatocellular carcinoma (HCC) ranks as the fifth most prevalent neoplasm in humans worldwide and stands as the primary cause of cancer-related mortality in specific regions [1]. This reality drives continuous research directed at formulating innovative therapies and diagnostic methods. The investigation into HCC mechanisms and the assessment of potential treatments heavily rely on animal models. Apart from spontaneous models involving animals like dogs and woodchucks, chemically induced rodent models take a central position in HCC research [2-5]. The administration of the carcinogenic and mutagenic compound Diethylnitrosamine (DEN) (CH3-CH2)2N-N=O) through parenteral or oral routes in experimental models animals is particularly utilized for its significant translational value in understanding the complex profile of aggressive forms of hepatocellular carcinoma (HCC) in humans [6]. DEN-induced hepatic tumors in rodents, through various mechanisms such as epigenetic and genetic changes, typically undergo a sequential progression. This starts with an initial phase of inflammation and necrosis, leading to long-term hepatocellular hyperplastic and dysplastic

changes, defined as "alteration foci," ultimately resulting in neoplastic transformation, including hepatocellular adenoma and carcinoma [7,8]. The hepatocellular "alteration foci" are identified as preneoplastic changes, characterized by their distinctive staining patterns on the conventional hematoxylin and eosin (HE) stain. While both acidophilic and basophilic foci are referenced in the context of hepatocellular alteration, in cases of HCC induced by DEN, the "basophilic foci" emerge as the primary preneoplastic phenotype changes in hepatocytes. Despite being mechanistically complex, the hepatocellular basophilic phenotype observed in alteration foci in DEN-induced HCC is attributed to metabolic shifts within cells. This reflects a progressive transition from anabolic to catabolic glucose metabolism, indicative of the Warburg effect, to sustain irregular cell proliferation [9]. A significant problem in comprehending the progression of chemically induced hepatocellular carcinomas in rodents is distinguishing early hepatocellular alterations that serve as precursors to carcinomas from those that are incidental or secondary phenomena [10]. The conventional method for defining and assessing hepatocellular alteration foci [11] traditionally relies on H&E staining. This classic staining technique, employed in all regulatory toxicological studies in animal models, utilizes hematoxylin ($C_{16}H_{14}O_6$) to stain anionic components (like DNA and RNA). Simultaneously, the xanthene pigment eosin Y ($C_{20}H_6Br_4Na_2O_5$) is applied to stain cationic compounds (such as proteins). Eosin Y binds electrostatically to the carboxylic and phenolic groups of arginine, histidine, lysine, and tryptophan residues [12]. Interestingly, Eosin is produced through the bromination of fluorescein, displaying a fluorescence photoactivity similar to its parent compound [13]. This unique fluorescence characteristic of eosin has been recently utilized as a diagnostic tool for quantifying liver injury [14]. Moreover, eosin serves as a fluorescent pH indicator, and certain derivatives are employed as reactive fluorescent labels. Eosin Y and fluorescein are applied as benchmarks for quantum yield, photosensitizing agents, laser dyes, and labeling biological specimens [15]. The present work aims to systemically assess the changes in the eosin fluorescence pattern in the preneoplastic, basophilic hepatic nodules obtained in a DEN-induced HCC murine model.2. Materials and Methods

Animals

The study involved 28 albino Swiss mice, young males, with an average weight of around 25g. Mice of the Swiss strain were purchased according to the regulations in force from the Iuliu Haţieganu UMF Animal Facilities Cluj-Napoca. These mice were housed in plastic cages with unrestricted access to food and water, under conditions of 22–23°C temperature, 55% humidity, and a 12-hour light/dark cycle. They were provided with standard pelleted rodent feed manufactured by Cantacuzino National Insitute for Medical-Military Research and Development. The research protocol received approval from DSVSA (National Veterinary Medicine Authority no. 267/12.07.2021). All procedures related to the use of laboratory animals adhered to the guidelines and European regulations outlined in EU Directive 2010/63/EU and Romanian law 43/2014.

Experimental design

The procedure for inducing liver carcinoma was modified from the method outlined by Sun et al. in 2012 [16], involving the following steps. The mice were assigned to four groups (Control, G1, G2, and G3), each with seven mice. Before each injection, mice were weighed to ensure accurate calculation of the diethylnitrosamine (DEN) dose. A single intraperitoneal dose of diethylnitrosamine at 100mg/kg was administered. The progression of hepatic alterations and HCC was monitored over time by systematically euthanizing animals at 2 months (G1), 5 months (G2), and 8 months (G3) post-DEN administration. The mice were euthanized with prolonged exposure to isoflurane. The spontaneous

deaths were not recorded during this experiment.The analysis of eosin fluorescence was carried out on the first and second sacrificed groups in which the presence of basophilic foci was observed..

Histopathological analysis

The liver was sampled for subsequent analysis and fixed in 10% formalin for 48 hours. Samples were fixed, dehydrated, and clarified in ethyl alcohol and xylene. Paraffin infiltration at 58°C for 5 hours was done, and 2 μm-thin sections were obtained. For staining, slides underwent xylene immersion, ethanol solutions, hematoxylin, and eosin Y. Dehydration included ethanol immersions, and clearing was done with xylene. Finally, Permount and coverslips were applied for microscopic observation of stained tissue sections. [17]. Histological examination of the samples was conducted using an Olympus BX51 microscope, and bright field images were captured using an Olympus SP350 digital camera, and processed using the Olympus cellSens software. The assessment of liver histopathology was performed based on the International Harmonization of Nomenclature and Diagnostic (INHAND) histological criteria standards for rodents [11.]*Chemical and Reagents*

N-Nitrosodiethylamine solution was purchased from Sigma (Lot# 049K1613). H&E staining kit was acquired from Abcam (H&E Staining Kit ab245880).

Confocal scanning laser microscopy (CSLM) analysis

Confocal fluorescent pictures were captured utilizing a Zeiss LSM 710 confocal laser scanning module installed on an Axio Observer Z1 Inverted Microscope. To visualize cell structures, a 488 excitation laser line was employed to detect Eosine (BP 493-625 nm emission). All pictures were taken with a Plan Apochromat 63× (1.4; oil immersion, DIC M27) Zeiss objective. Standard ZEN software provided by the Zeiss system manufacturer was utilized for image merging, processing, and analysis. Fluorescence values were denoted in arbitrary units (AU).

Eosine quantification by CLSM

The assessment of Eosine expression in the liver followed a methodology similar to our previous work [18]. Quantitative analysis of the confocal images was automated using the point-by-point fluorescence quantification functions within the ZEN software. To ensure consistent quantification conditions and maintain high reproducibility, CLSM image acquisition was standardized and upheld throughout the experiment (acquisition time 30 s, lasers' output power 20%, pinhole diameter 53 μm, master gain 420, digital gain 15 Each image section measured 512 × 512 pixels (135× 135μm), covering an area of 18.225 μm² for every scanned microscopic field. Mean fluorescence was assessed on five basophilic foci by examining two fields (obx63) per focus (totaling 10 fields with basophilic foci). In a similar matter, the perilesional liver for each basophilic focus was assessed in 2 histological fields from the same histological slides. Additionally, measurements on 10 fields from an uninjected mouse serving as the control were conducted *Statistical analysis*

Statistical evaluations were conducted utilizing RStudio version 4.3.1. For datasets distribution it was used the Shapiro-Wilk normality test. To assess the intensity of the Eosine in the Kruskal-Wallis and with Dunn's post-hoc analysis with Bonferroni correction was utilized.

3. Results

Modifications associated with DEN administration were noted in the second and third groups, occurring approximately 5 and 8 months following administration. Pathologically, the first group (sacrificed at 2 months) showed no visible macroscopic changes, while the second group displayed distinct masses in four out of seven examined livers. The masses were white-beige, well-demarcated, measuring up to 3 mm, with a multifocal or multifocal-coalescing arrangement, distributed in all hepatic lobes (up to 15 masses /liver). Similarly, in the third experimental group, masses were detected in five out

of seven examined livers. In this group, the masses measure up to 1 cm, maintaining the same multifocal or multifocal-coalescing arrangement as in group 3. Intratumoral necrosis was occasionally noted in the masses of this group. Histologically, the basophilic foci, (randomly distributed and predominantly observed within the initial two groups and evaluated in the context of this experiment), consist of well-defined, nodular, circular, un-encapsulated lesions characterized by hepatocytes organized in interconnected cord-like structures, exhibiting minimal cellular polymorphism. These foci prominently displayspecific tinctorial staining patterns and granularity. The global tissue architecture within the basophilic foci experiences a moderate level of disruption**.** The cellular components in these foci may appear darker (basophilic) compared to adjacent tissues. The majority of hepatocytes within the basophilic foci exhibit a prominent abundance of granular and intensely basophilic cytoplasm. Noteworthy histological features encompass nuclear alterations, including occasional nuclear enlargement, and heightened chromatic intensity (hyperchromasia). The nuclei within these foci reveal vacuolated chromatin, and in some instances, the presence of 1-2 distinct basophilic nucleoli. These observed histopathological characteristics collectively contribute to the comprehensive understanding of the cellular and nuclear alterations inherent in basophilic following DEN administration (Figure 1 image A, B, C).

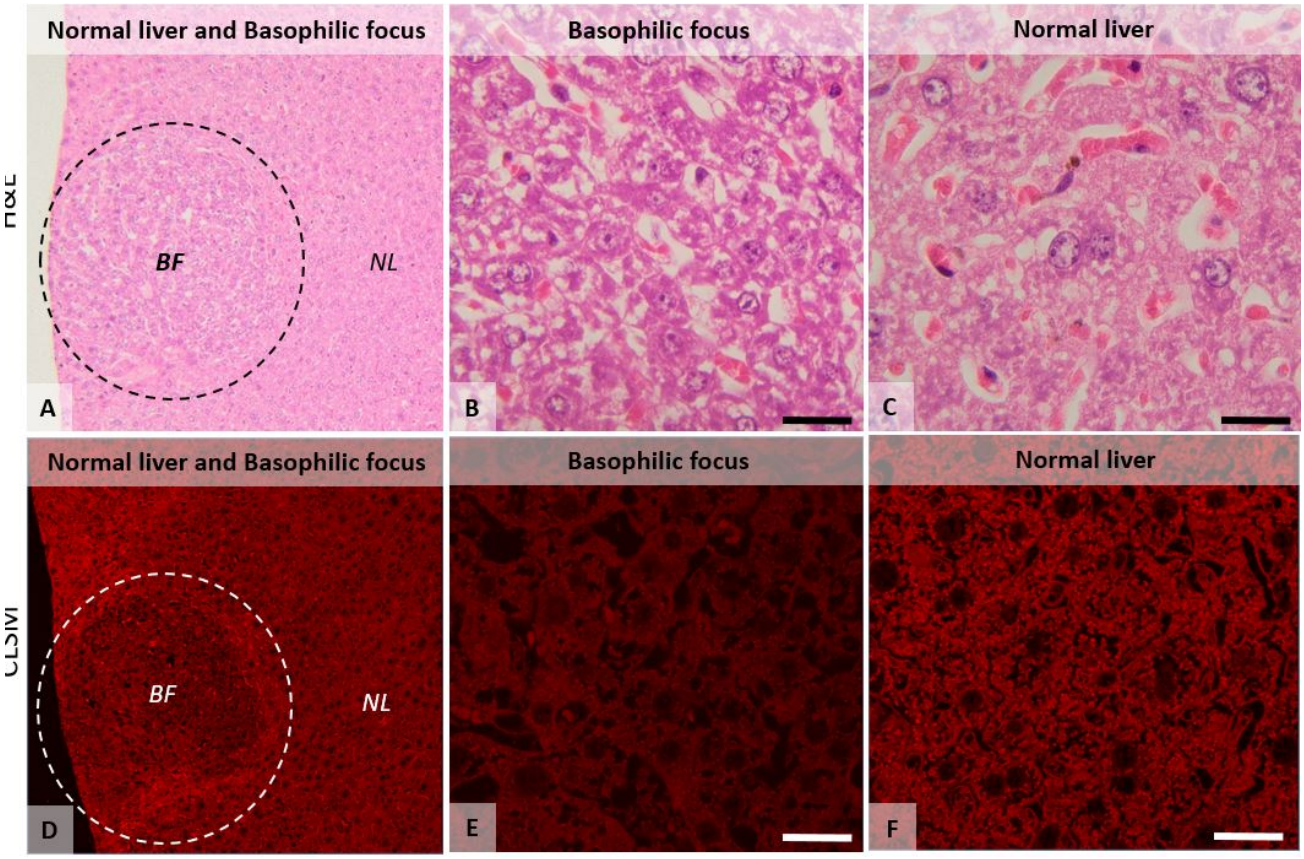

Figure. 1. Histological images (A, B and C) and Confocal laser (D, E, and F) of the mice liver, comparing the hepatocellular preneoplastic basophilic alteration foci (BF) with the normal liver parenchyma (NL). Image A. Histological micrographs showing a well-demarcated, subscapular hepatocellular basophilic focus (BF), characterized by tortuously arranged hepatic chords, with hepatocytes showing increased cytoplasmic basophilia relative to adjacent normal parenchyma, without significant compression of the bordering tissue. Image B. The hepatocytes of the basophilic focus, are

characterized by bands of localized, clumped basophilic bodies in the peripheral cytoplasm with clear intervening areas ("tigroid" pattern). **Image B.** Hepatocytes from the control group, showing normal patterns of cytoplasmic staining. Image D. Confocal images of the basophilic focus (BF) presented in image A, showing reduced overall fluorescence compared with the adjacent hepatic tissue (NL). Image E. Confocal images of the hepatocytes from the basophilic focus, showing a reduced cytoplasmic fluorescence compared with the fluorescence observed in the adjacent, normal liver (image F). CLSM objective 10 (image D) and x63×/1.4 Oil Plan Apochromatic objective (images E and F); H&E images, ob x10 (images A) and x 100 (images B and C). Scale bar=20μm.

Concerning the CLSM manifestation of Eosin expression, a discernible reduction in fluorescence intensity was evident when comparing normal hepatic tissue to basophilic foci. Within the confines of a morphological normal liver, the fluorescence intensity of Eosin exhibits a visibly elevated profile as opposed to the diminished Eosin fluorescence encountered within basophilic foci, thereby indicating a discernible alteration in Eosin fluorescence within the latter. (Figures 1 Image D,E,F, and Figure 2,).

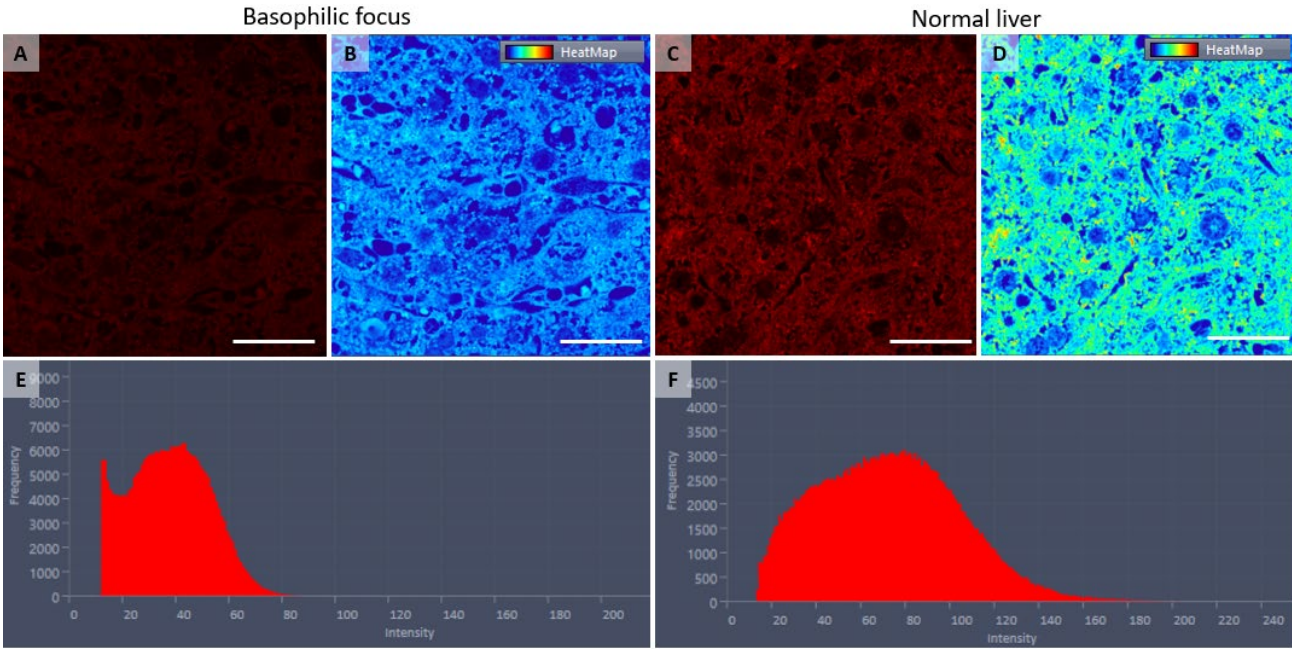

Figure. 2. Confocal laser scanning microscopy micrographs of liver tissue, presenting the basophilic foci (images A and B) and their fluorescence spectra (image E) compared with the normal adjacent liver parenchyma (images C, and D) and its fluorescent spectra (image F). The fluorescence intensity distribution histograms (images E and F) show the altered expression of the Eosin/fluorescein within the hepatocytes of the basophilic foci compared with normal hepatic tissue. The Eosin/fluorescein expression = red channel. Images B and D compare the fluorescence expression of Eosin/fluorescein as a heatmap in the basophilic foci (B) compared with normal tissue hepatic (D). Warmer colors indicate higher Eosin/fluorescein expression intensities. 63×/1.4 Oil Plan Apochromate objective.

Statistically, the Shapiro-Wilk test indicates that the data for all groups are normally distributed. Posthoc Dunn's test with Bonferroni correction revealed significant differences between the "Basophilic foci" group and both the "Normal liver (control)" and "Normal liver (perilesional)" groups, but not between the latter two. Specifically, the comparison of basophilic foci with normal liver (control) yielded a P-value of 0.00485, while the comparison with normal liver (perilesional) also resulted in a P-value of 0.00485. Despite the data's normality, the Kruskal-Wallis test revealed significant differences among the groups' medians, with post-hoc Dunn's test confirming significant disparities between the "Basophilic foci" group and both "Normal liver (control)" and "Normal liver (perilesional)" groups, albeit not between the latter two.

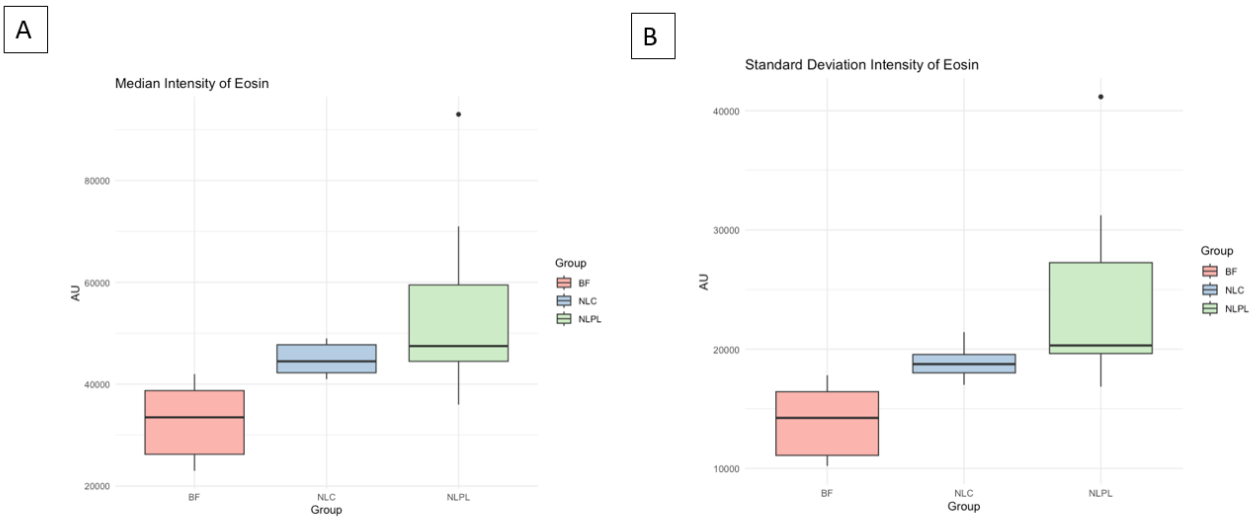

Figure 3. Image A. represets Comparative Analysis of Eosin Median Intensity Across Liver Tissue Conditions in Mice. Box plot A representation of the median intensity of eosin staining across three distinct liver tissue conditions in mice: Basophilic foci (BF), Normal liver (control, NLC), and Normal liver (perilesional, NLPL). The eosin median intensity is markedly lower in Basophilic foci (BF) compared to Normal liver (control, NLC), suggesting a diminished central tendency of eosin intensity in BF. In contrast, the median intensity in Normal liver (perilesional, NLPL) is elevated, indicating a higher eosin affinity or increased density of staining in perilesional compared to control tissues. These observations may reflect differential eosinophilic activity or structural variations among the hepatic conditions examined. Image B represents Variability in Eosin Staining Intensity Among Liver Tissue Conditions in Mice. This box plot illustrates the variability, as measured by standard deviation, of eosin staining intensity within three different liver tissue conditions in mice: Basophilic foci (BF), Normal liver (control, NLC), and Normal liver (perilesional, NLPL). The standard deviation is substantially lower in the Basophilic foci (BF) group, suggesting more homogeneity in staining intensity, whereas the Normal liver (perilesional, NLPL) exhibits a higher standard deviation, indicating greater variability in eosin uptake or distribution. The Normal liver (control, NLC) shows intermediate variability. These differences in standard deviation may imply distinct histological characteristics or differential responses to staining due to the underlying pathology of the tissue."

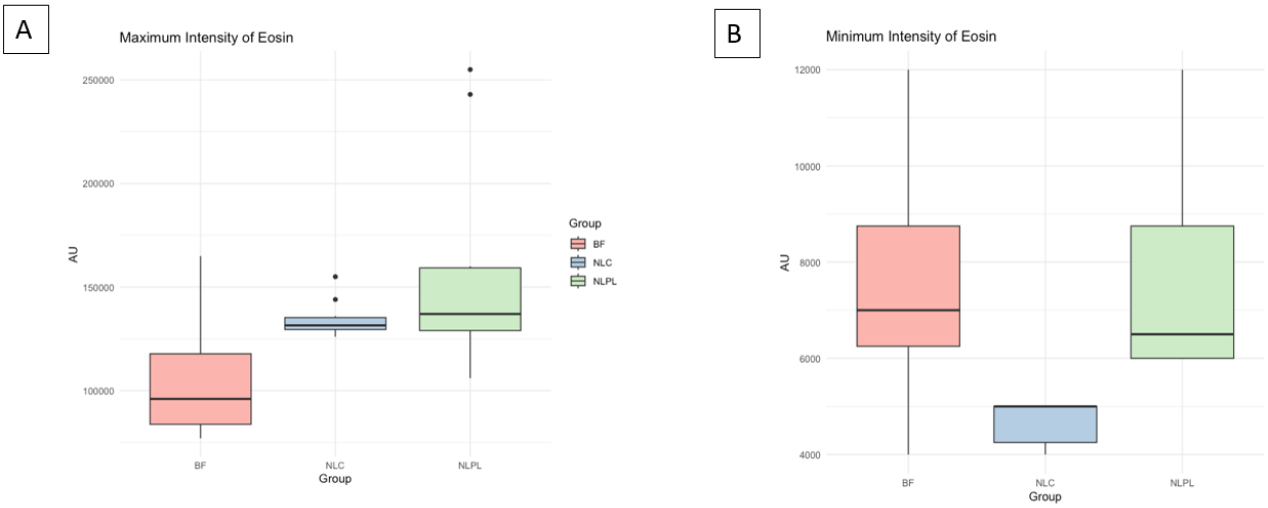

Figure 4. Image A represents Evaluation of Maximum Eosin Staining Intensity in Diverse Liver Tissue States in Mice. The box plot showcases the maximum intensity of eosin staining within three liver tissue states: Basophilic foci (BF), Normal liver (control, NLC), and Normal liver (perilesional, NLPL). The Basophilic foci (BF) group exhibits a lower range of maximum intensity, suggesting a restricted eosin presence or a lesser degree of staining peak. In contrast, the Normal liver (perilesional, NLPL) displays a substantially higher maximum intensity, indicating intense eosinophilic engagement or staining concentration, potentially reflective of heightened inflammatory or morphological alterations in perilesional tissue**.** Image B represents Assessment of Minimum Eosin Staining Intensity Across Varied Liver Conditions in Mice. The box plot depicts the minimum intensity of eosin staining for Basophilic foci (BF), Normal liver (control, NLC), and Normal liver (perilesional, NLPL) conditions in murine hepatic tissue. The minimum intensity levels are notably higher in the Basophilic foci (BF) and Normal liver (perilesional, NLPL) groups compared to the Normal liver (control, NLC), indicating a greater baseline level of eosin staining in these conditions. This could suggest a floor effect of eosinophil infiltration or binding affinity in the BF and NLPL tissues."

4. Discussion

In rodent toxicity experiments involving specific xenobiotics, cellular changes known as basophilic foci are observable alterations in liver tissue. These changes, visible under stains like H&E, reveal unique characteristics in terms of cell type, staining patterns, and texture, offering insights into liver morphological variations linked to hepatocarcinogenesis [19]. Basophilic foci typically appear as circular or ovoid lesions, differing noticeably from normal liver tissue in staining reactions and cellular appearance. The differentiation of basophilic foci types, based on staining attributes, hepatocyte size, and texture, aids in understanding the complex cellular transformations within the liver. While maintaining lobular architecture, these foci may vary in portal areas and central veins depending on their size. Compression of sinusoids within the foci can affect the detection of typical parenchymal plates, and increased cellular numbers may lead to the development of tortuous hepatic cords [11].

Early stages of hepatocarcinogenesis induced by DEN administration involve molecular changes highlighted by Watanabe et al. [20], revealing mRNA networks associated with cancer-related genes, cell cycle regulation, and cell death. The progression from pre-neoplastic foci to distinct phenotypes such as basophilic, eosinophilic, or clear cell foci is linked to metabolic turnover, with specific molecular events driving this transition. Elevated insulin growth factor 2 (IGF-2) levels and downstream signaling play key roles in shaping glycogen storage phenotypes, ultimately leading to the basophilic phenotype [21]. Initially, exposure to DEN elevates insulin IGF-2 levels, initiating downstream signaling that reduces glucose-6-phosphatase (G6Pase) activity, resulting in glycogen storage phenotypes. Moreover, IGF signaling activates the Ras/Raf mitogen-activated signaling cascade, promoting cell proliferation [22]. Over time, the foci transition from anabolic to catabolic glucose metabolism to support cell proliferation, culminating in the development of the basophilic phenotype. Some altered hepatocyte foci (AHF) exhibit mutations in Hras and Braf oncogenes, potentially providing a growth advantage, as these molecular alterations are more frequently observed in late-stage neoplastic lesions [23]. Braf mutations induce ERK1/Akt hyperphosphorylation, leading to the induction of pro-survival/pro-proliferative complement component C5/C5a in basophilic foci [24]. Consequently, AHF are generally considered putative preneoplastic lesions in chemically induced models, although the full significance of morphologically similar lesions in human hepatocarcinogenesis remains incompletely understood.

The development of hepatocellular carcinoma (HCC), involving initiation, promotion, and progression, is influenced by interactions among genetic, epigenetic, and environmental factors. Initiation often arises from genetic mutations induced by various carcinogens, such as aflatoxin, hepatitis B or C viruses, alcohol, metabolic disorders, and inflammation, causing DNA damage [26,27]. Chronic liver diseases create a conducive environment for HCC promotion, leading to the accumulation of genetic abnormalities and preferential selection of growth-advantaged cells. Subsequent genetic modifications in the promotion phase activate oncogenes, facilitate cell growth, and deactivate tumor suppressor genes, collectively contributing to unregulated cell multiplication [28,29]. As tumors progress, angiogenesis is triggered for continued growth, enabling infiltration into adjacent tissues and dissemination to distant organs, involving alterations in adhesion, migration, and invasion. HCC strategically evades the immune system, avoiding detection and elimination by the body's innate defense mechanisms [30,31].

Traditional staining methods, like hematoxylin-eosin, and selective fluorescence reactions, notably with eosin Y, provide valuable tools for histological examination. Eosin Y's versatility extends beyond histology, serving as a fluorescent dye for various cellular structures, highlighting its utility in diverse applications [13,32]. By comparing optical images of basophilic alteration foci stained by H&E with their confocal fluorescence spectra, a correlation between the loss of fluorescence intensity and loss of hepatocyte tinctorial affinity for eosin (defined as "basophilia") is observed. These findings are significant from a diagnostic perspective, employing confocal laser scanning microscopy (CLSM) as a tool in toxicological pathology, aiding in establishing the link between tinctorial changes of basophilic foci (preneoplastic changes) and their fluorescence spectral shifts

5. Conclusions

Following this study, we managed to demonstrate the presence of alterations in the fluorescence spectrum of eosin when bound to proteins in both normal and tumoral liver tissues. This highlights how fluorescence spectroscopy can potentially complement histopathological observations and unveil information that aligns with classical H&E staining methods. Given its inherent

sensitivity to changes in the biomolecular composition across diverse cell and tissue types, fluorescence microscopy can offer information surpassing that of individual conventional diagnostic techniques. Anticipating widespread applications, we envision that this fluorescence imaging approach will prove valuable in diverse fields, including cell biology, biomedical analysis and diagnosis, and the chemical identification of various components within cells and tissues.

Author Contributions: RP, AFT, and TM carried out the HCC protocol. RP and AFT carried out the histological and CLSM assessment and drafted and reviewed the manuscript. DH was involved in the data analysis and statistics. CC and LM reviewed the manuscript. All authors read and approved the final manuscript.

Funding: The authors wish to acknowledge funding granted by the National Authority for Scientific Research and Innovation Romania, CNCS-UEFISCDI, cod PN-III-P2-2.1-PED-2021-0073 and PN-III-P2-2.1-PED-2019-0997.

Institutional Review Board Statement: The experimental protocol has been approved by DSVSA (National Veterinary Medicine Authority no. 267/12.07.2021). All procedures involving the use of laboratory animals followed the guidelines and European norms 337 established by EU Directive 2010/63/EU and Romanian law 43/2014

Data Availability Statement: The data that support the findings of this study are available from the Department of Veterinary Pathology, University of Agriculture Science and Veterinary Medicine. Data are, however available from the authors upon reasonable request and with the permission of the Department of Veterinary Pathology, University of Agriculture Science and Veterinary Medicine.

Acknowledgments: Not applicable

Conflicts of Interest: The authors declare no conflict of interest.

References

1. Bruix, Jordi, Loreto Boix, Margarita Sala, and Josep M. Llovet. "Focus on hepatocellular carcinoma." Cancer cell 5, no. 3 (2004): 215-219.
2. Zhang, Hui Emma, James M. Henderson, and Mark D. Gorrell. "Animal models for hepatocellular carcinoma." Biochimica et Biophysica Acta (BBA)-Molecular Basis of Disease 1865, no. 5 (2019): 993-1002.
3. Li, Yan, Zhao-You Tang, and Jin-Xuan Hou. "Hepatocellular carcinoma: insight from animal models." Nature reviews Gastroenterology & hepatology 9, no. 1 (2012): 32-43.
4. Li, Enya, Li Lin, Chia-Wei Chen, and Da-Liang Ou. "Mouse models for immunotherapy in hepatocellular carcinoma." Cancers 11, no. 11 (2019): 1800.
5. Suresh, Manasa, and Stephan Menne. "Application of the woodchuck animal model for the treatment of hepatitis B virus-induced liver cancer." World Journal of Gastrointestinal Oncology 13, no. 6 (2021): 509.
6. Romualdo, Guilherme Ribeiro, Kaat Leroy, Cícero Júlio Silva Costa, Gabriel Bacil Prata, Bart Vanderborght, Tereza Cristina Da Silva, Luís Fernando Barbisan et al. "In vivo and in vitro models of hepatocellular carcinoma: current strategies for translational modeling." Cancers 13, no. 21 (2021): 5583.
7. Uehara, Takeki, Igor P. Pogribny, and Ivan Rusyn. "The DEN and CCl4-induced mouse model of fibrosis and inflammation-associated hepatocellular carcinoma." Current protocols in pharmacology 66, no. 1 (2014): 14-30.
8. Kurma, Keerthi, Olivier Manches, Florent Chuffart, Nathalie Sturm, Khaldoun Gharzeddine, Jianhui Zhang, Marion Mercey-Ressejac et al. "DEN-induced rat model reproduces key features of human hepatocellular carcinoma." Cancers 13, no. 19 (2021): 4981.
9. Suzuki, Hideo, Motoyuki Kohjima, Masatake Tanaka, Takeshi Goya, Shinji Itoh, Tomoharu Yoshizumi, Masaki Mori et al. "Metabolic alteration in hepatocellular carcinoma: mechanism of lipid accumulation in well-differentiated hepatocellular carcinoma." Canadian Journal of Gastroenterology and Hepatology 2021 (2021): 1-13.
10. Goldfarb, Stanley, Thomas D. Pugh, Hirofumi Koen, and Yu-Zhu He. "Preneoplastic and neoplastic progression during hepatocarcinogenesis in mice injected with diethylnitrosamine in infancy." Environmental Health Perspectives 50 (1983): 149-161.
11. Thoolen, Bob, Robert R. Maronpot, Takanori Harada, Abraham Nyska, Colin Rousseaux, Thomas Nolte, David E. Malarkey et al. "Proliferative and nonproliferative lesions of the rat and mouse hepatobiliary system." Toxicologic pathology 38, no. 7_suppl (2010): 5S-81S.
12. Chan, John KC. "The wonderful colors of the hematoxylin–eosin stain in diagnostic surgical pathology." International journal of surgical pathology 22, no. 1 (2014): 12-32

13. Acharya, Seema, and Babulal Rebery. "Fluorescence spectrometric study of eosin yellow dye–surfactant interactions." Arabian Journal of Chemistry 2, no. 1 (2009): 7-12.
14. Ali, Hamid, Safdar Ali, Maryam Mazhar, Amjad Ali, Azra Jahan, and Abid Ali. "Eosin fluorescence: A diagnostic tool for quantification of liver injury." Photodiagnosis and Photodynamic Therapy 19 (2017): 37-44.
15. De Rossi, Andiara, Lenaldo B. Rocha, and Marcos A. Rossi. "Application of fluorescence microscopy on hematoxylin and eosin-stained sections of healthy and diseased teeth and supporting structures." Journal of oral pathology & medicine 36, no. 6 (2007): 377-381.
16. Sun, Hua, Linghong Yu, Huailing Wei, and Gengtao Liu. "A novel antihepatitis drug, bicyclol, prevents liver carcinogenesis in diethylnitrosamine-initiated and phenobarbital-promoted mice tumor model." Journal of Biomedicine and Biotechnology 2012 (2012).
17. Cardiff, Robert D., Claramae H. Miller, and Robert J. Munn. "Manual hematoxylin and eosin staining of mouse tissue sections." Cold Spring Harbor Protocols 2014, no. 6 (2014): pdb-prot073411
18. Clichici, Simona, Alexandru Radu Biris, Flaviu Tabaran, and Adriana Filip. "Transient oxidative stress and inflammation after intraperitoneal administration of multiwalled carbon nanotubes functionalized with single strand DNA in rats." Toxicology and Applied Pharmacology 259, no. 3 (2012): 281-292.
19. Harada, Takanori, Robert R. Maronpot, Gary A. Boorman, Richard W. Morris, and Katherine A. Stitzel. "Foci of cellular alteration in the rat liver: a review." Journal of Toxicologic Pathology 3, no. 2 (1990): 161-188.
20. Watanabe, Takashi, Gotaro Tanaka, Shuichi Hamada, Chiaki Namiki, Takayoshi Suzuki, Madoka Nakajima, and Chie Furihata. "Dose-dependent alterations in gene expression in mouse liver induced by diethylnitrosamine and ethylnitrosourea and determined by quantitative real-time PCR." Mutation Research/Genetic Toxicology and Environmental Mutagenesis 673, no. 1 (2009): 9-20.
21. Lahm, Harald, Katinka Gittner, Ottheinz Krebs, Lisa Sprague, Erhard Deml, Doris Oesterle, Andreas Hoeflich, Rüdiger Wanke, and Eckhard Wolf. "Diethylnitrosamine induces long-lasting re-expression of insulin-like growth factor II during early stages of liver carcinogenesis in mice." Growth hormone & IGF research 12, no. 1 (2002): 69-79.
22. Buchmann, Albrecht, Züleyha Karcier, Benjamin Schmid, Julia Strathmann, and Michael Schwarz. "Differential selection for B-raf and Ha-ras mutated liver tumors in mice with high and low susceptibility to hepatocarcinogenesis." Mutation Research/Fundamental and Molecular Mechanisms of Mutagenesis 638, no. 1-2 (2008): 66-74
23. Connor, Frances, Tim F. Rayner, Sarah J. Aitken, Christine Feig, Margus Lukk, Javier Santoyo-Lopez, and Duncan T. Odom. "Mutational landscape of a chemically-induced mouse model of liver cancer." Journal of hepatology 69, no. 4 (2018): 840-850.
24. Parekh, Palak, and K. V. K. Rao. "Overexpression of cyclin D1 is associated with elevated levels of MAP kinases, Akt and Pak1 during diethylnitrosamine-induced progressive liver carcinogenesis." Cell biology international 31, no. 1 (2007): 35-43.
25. Dragan, Y. P., L. Sargent, Y-D. Xu, Y-H. Xu, and H. C. Pitot. "The initiation-promotion-progression model of rat hepatocarcinogenesis." Proceedings of the Society for Experimental Biology and Medicine 202, no. 1 (1993): 16-24.
26. Severi, Tamara, Hannah Van Malenstein, Chris Verslype, and Jos F. Van Pelt. "Tumor initiation and progression in hepatocellular carcinoma: risk factors, classification, and therapeutic targets." Acta Pharmacologica Sinica 31, no. 11 (2010): 1409-1420.
27. Pitot, Henry C., and Alphonse E. Sirica. "The stages of initiation and promotion in hepatocarcinogenesis." Biochimica et Biophysica Acta (BBA)-Reviews on Cancer 605, no. 2 (1980): 191-215.
28. Dapito, Dianne H., Ali Mencin, Geum-Youn Gwak, Jean-Philippe Pradere, Myoung-Kuk Jang, Ingmar Mederacke, Jorge M. Caviglia et al. "Promotion of hepatocellular carcinoma by the intestinal microbiota and TLR4." Cancer cell 21, no. 4 (2012): 504-516.
29. Domínguez-Malagón, Hugo, and Silvia Gaytan-Graham. "Hepatocellular carcinoma: an update." Ultrastructural pathology 25, no. 6 (2001): 497-516.
30. Ogunwobi, Olorunseun O., Trisheena Harricharran, Jeannette Huaman, Anna Galuza, Oluwatoyin Odumuwagun, Yin Tan, Grace X. Ma, and Minhhuyen T. Nguyen. "Mechanisms of hepatocellular carcinoma progression." World journal of gastroenterology 25, no. 19 (2019): 2279.
31. Singh, Amit Kumar, Ramesh Kumar, and Abhay K. Pandey. "Hepatocellular carcinoma: causes, mechanism of progression and biomarkers." Current chemical genomics and translational medicine 12 (2018): 9.
32. Herculano, L. S., L. C. Malacarne, V. S. Zanuto, G. V. B. Lukasievicz, O. A. Capeloto, and N. G. C. Astrath. "Investigation of the photobleaching process of eosin Y in aqueous solution by thermal lens spectroscopy." The Journal of Physical Chemistry B 117, no. 6 (2013): 1932-1937.

CVJ CLUJ VETERINARY JOURNAL

Review

Comprehensive Evaluation of Direct Methods for Failure of Passive Transfer Diagnosis in Neonatal Calves

Dragoș Adrian Popescu [1], Florin Petrișor Posastiuc [1, 2, *], Nicolae Tiberiu Constantin [1, 3], Crina Raluca Andrei [1,3], Florina Marian[4] and Mario Darius Codreanu [1]

[1] Faculty of Veterinary Medicine, University of Agronomic Sciences and Veterinary Medicine, Bucharest, Romania
[2] Faculty of Veterinary Medicine, Ghent University, Merelbeke, Belgium
[3] Research and Development Institute for Bovine Balotești, Balotești, Romania
[4] Faculty of Veterinary Medicine, University of Agricultural Sciences and Veterinary Medicine Cluj-Napoca, Romania
*Correspondence: florin.posastiuc@ugent.be

Abstract: Failure of Passive Transfer (FPT) is a critical concern in neonatal calves, marked by inadequate maternal immunoglobulin transmission due to the synepitheliochorial placenta. This leads to heightened disease prevalence, significantly impacting calf health and imposing substantial economic burdens. The prevalence of FPT varies globally, with studies reporting incidence rates ranging from 13% to 41%, one of the explanations for such high variability being the use of different methods and non-adapted thresholds. Efficient diagnostic methodologies are essential to address this challenge, with ongoing exploration of alternative approaches beyond the established gold standard of radial immunodiffusion (RID). This review critically evaluates the available direct methods for FPT assessment gathering the most recent data on both established methods such as enzyme-linked immunosorbent assay (ELISA) and innovative methodologies such as immunoturbidimetry, split trehalase IgG assay (STIGA), ionization techniques (IT), mass spectrometry (MS), proteomics, and infrared spectroscopy (IS) with attenuated infrared spectroscopy (ATR). Exploring beyond conventional practices is vital for enhancing diagnostic accuracy and addressing the complexities of FPT in calf health management.

Keywords: failure of passive transfer; radial immunodiffusion; calf management; immunoglobulins, total serum protein

Received: 19 January 2024
Accepted: 11 February 2024
Published: 9 April 2024

DOI:10.52331/bkynge51

1. Introduction

The synepitheliochorial placenta in cows, with its capacity to separate maternal and fetal blood supplies, effectively inhibits the *in-utero* transmission of protective immunoglobulins [1]. Consequently, calves are born with insufficient immunity, making them highly dependent on colostrum intake [2].

The colostrum incorporates blood serum components [3], such as immunoglobulins, mainly IgG [4]. The secretion is transitory, and the antibody levels gradually decline over time, reaching very low levels 24 hours after birth [5]. Antibodies from the colostrum are absorbed by epithelial cells in the small intestine, particularly in the jejunum and ileum, via pinocytosis [1]. Afterward, immunoglobulins are transferred to the main lymphatic tissue components, entering systemic circulation via the thoracic duct [1]. Unfortunately, the pinocytotic mechanism fully ceases the transfer of large molecules after the first 24 hours [2]. Beyond

this point, additional intake of colostral immunoglobulins can offer local intestinal protection but does not contribute to the calf's overall systemic protection [2].

The neonatal calf's inability to absorb sufficient colostral immunoglobulins during the initial hours of life leads to a failure in passive transfer (FPT) [6]. FPT was associated with high economic losses [6] and increased disease prevalence [7, 8]. Dairy calves experiencing FPT were twice as likely to develop diarrhea and necessitate antibiotic therapy before weaning [9-12]. Various thresholds for serum IgG were contemplated based on the animal category. In the case of the mentioned dairy calves, the designated cut-off value for FPT was established at 10 g/L, with lower levels correlating to elevated rates of mortality and morbidity [2, 13]. The situation appears to be more alarming in beef cattle, with the established threshold set at 24 g/L [14]. Beef calves with serum IgG levels below 24 g/L may be 1.6 times more susceptible to death compared to those with higher IgG values [14]. Other studies report even more concerning findings, considering a mortality rate 2.7 times higher before weaning, under the same circumstances [15]. An alternative approach is represented by the measurement of serum total protein concentrations (STPC), considering a threshold of 52 g/dL as equivalent to IgG levels inferior to 10 g/L [16]. These results motivated a series of researchers to orient their work to different treatment and prophylactic alternatives, such as the use of hyperimmune plasma [17], along with non-enriched blood products [18].

The prevalence of FPT was intensively studied in the last decade different prevalence rates being recorded, ranging from 13% [19] to 33% [20] and even 46.5% [21].

However, these results may be method-dependent, and several direct or indirect techniques for FPT assessment being scrutinized such as: Brix refractometry (BR), gamma-glutamyl transferase activity, zinc sulfate turbidity test, enzyme-linked immunosorbent assay (ELISA), radial immunodiffusion (RID), electrophoresis, capillary electrophoresis (CE), turbidimetric immunoassays, Split trehalase IgG assay (STIGA), Ionization techniques (IT) and mass spectrometry (MS), Infrared spectroscopy (IS) with Transmitted & Attenuated Infrared Spectroscopy (ATR) and proteomics. The suitability of various methods is still a topic of discussion, with some techniques proving more fitting for on-site calf applications but potentially lacking in sensitivity. The aim of this paper is to gather the most recent information on the direct methods available for FPT evaluation, as indirect methods have been recently reviewed [22].

2. Direct methods for FPT evaluation

2.1 Radial immunodiffusion (**RID) – golden standard for FPT assessment**

Currently, the reference test for IgG determination is RID but even this method has several drawbacks being impractical for clinical use. This belief is backed up by the relatively high cost, the need for skilled operators, and a specifically equipped laboratory [23]. In addition, this method implies working on low-volume assays [23], the reagents and required antibodies having limited durability [24]. Results are usually obtained in 18 or 24 hours after admitting the samples to work, the measurements applied to the precipitation zones being time-consuming [25, 26]. In addition, if the coefficient of variation between the samples exceeds 10%, carrying out the test at least twice may be recommended [27, 28].

However, the method described by Mancini et al. (1965) with its variations has been extensively applied for different purposes in immunoglobulin quantitative studies [29, 30].

In contemporary literature, the use of RID is acknowledged as a valuable approach for assessing IgG levels in bovines. Findings indicate that, in certain instances, results obtained through RID may diverge from those obtained through alternative methods such as ELISA or electrophoresis [29] [31-33]. Gathering four different analytical methods of assessing FPT (ELISA, electrophoresis, and refractometry), a German research group used RID as gold standard, with results from the other procedures being referred to the latter [32]. Even if the same authors considered that the results from the other techniques are highly correlated to the standard, they stated that a true quantitative comparison between RID and ELISA or electrophoresis is inadequate. Moreover, the demand to adapt the thresholds for every assay depending on the sample type, serum or plasma, has been pinpointed.

Beyond several studies comparing other methods to the RID IgG results in order to assess the applicability of different techniques [31-34], there is also data available regarding the comparison between commercial RID kits [35]. Thus, it has been ratified that even different available kits may be subject to variability. Accordingly, it was considered that a three internal standard kit formulation may reveal with higher precision IgG levels compared to a single RID kit [35].

2.2. Immunoturbidimetry

Turbidimetric immunoassays have been recently developed and proposed for different applications such as acute phase protein determination in swine [36] and IgG serum evaluation in bovines [37]. Published research has indicated the potential for rapid analysis, with absorbance readings through spectrophotometry yielding results within 10 minutes [37]. This became achievable after adapting the original method [38] to the use of a portable laboratory instrument for in-farm applications [37]. The suitability of the method was backed up by analytical survey. Based on regression analysis, the automated immunoassay results closely paralleled those obtained by RID, with a correlation coefficient of 0.988,and a coefficient of determination value between immunoturbidimetry and RID of 0.98 [37].

Point-of-care assays based on turbidimetry have proven good sensitivity and specificity [39]. Based on these premises other authors compared bovine specific turbidimetric assays to several techniques for FPT evaluation [40]. However, the turbidimetric immunoassays were deemed to be only fairly correlated to RID, and a large bias was determined between the two [40].

Further studies have analyzed the use of turbidimetry-based calf-side tests [41, 42]. The high efficiency of the above-mentioned for FPT diagnosis in calves is considered relatively sensitive and suitable for initial screening [42]. Moreover, to reduce processing time requirements, further validation of whole blood tests, through semiquantitative IgG determinations were proposed [41]. Unfortunately, the method did not prove to be sufficiently accurate for immune status assessments, exhibiting a 77% sensitivity and 44% specificity compared to RID [41].

2.3. Split trehalase IgG assay (STIGA)

A novel detection platform based on a glycolytic enzyme, trehalase respectively, was recently proposed [43].

Further research has proven the possibilities of measuring IgG levels in more than one species, through the use of three bacterial immunoglobulin binding proteins (protein G, protein A, and

protein L) [44]. Thus, the use of this method has been ratified in a large number of species, with activation being detected in almost all tested situations, except for birds [44].

In bovines, the results are spectacular, at an absorbance optical density of 0.2 sensitivity rate reaching 77.8% and specificity 98.2% [27]. Moreover, a blinded trial has been carried out, with high correlation values being observed when compared to RID for both colostrum and serum [27]. In this manner, the authors managed to obtain 100% sensitivity and 94.7% specificity, for FPT diagnosis when using serum samples [27].

The advantages of the method have been further depicted, highlighting its high efficiency in the direct detection of IgG levels through a single-step analysis [27]. In addition, STIGA provides swift results, requiring only 90 minutes as opposed to longer time intervals needed for RID (up to 48 h) [27, 45]. From an economic perspective, STIGA is less expensive due to the lower production costs of the reagents compared to RID, less laborious, and suitable for automatization [27]. The latter statement was backed up by the user-friendly format that could be optimized for field testing, STIGA$^{FIELD\ ®}$, which rendered the same high correlation between its results and the ones obtained by RID [27].

2.4. Enzyme-linked immunosorbent assay (ELISA)

ELISA is broadly used for different means regarding veterinary practice. Among its diverse applications, this technique has been utilized extensively to determine IgG levels in colostrum, plasma, and sera [31, 33] [46-49].

Additionally, as a direct, laboratory-based method [49], ELISA proved to be a good alternative to RID in terms of costs [33]. Comparative studies have shown that the level of agreement between the two stated methods is considered to be high (94%), this assay being suitable for both screening and diagnosis of FPT. Another study gathering 206 Holstein-Friesian calves, compared ELISA to other methods while using different sample types. The Pearson correlation coefficients between the latter and RID remained at a high level (0.9) when serum was analyzed [32]. Also, a high correlation has been established between CE and ELISA (0.89), with the same authors proposing method-dependent cut-off values (5.4 mg IgG/mL for ELISA and 6.9 mg IgG/mL for CE) [32]. In contrast to these results, other authors were able to display only a relatively weak correlation between ELISA and RID ($r= 0.59$, $P < 0.01$), when using plasma samples [33], their results being closer to the ones obtained through immunoturbidimetry, also consistently lower than the RID values [50]. However, not only one statement rendering the comparison between such methods (RID vs ELISA) as being inadvisable, has been formulated [31, 33]. The main reason for the hindmost statement refers to the poor agreement between the assays [31].

A rapid test based on a competitive immunoassay was also compared to ELISA using 277 samples obtained from calves housed in 16 farms [51]. The quick method and ELISA were highly significantly correlated but the strength of the correlation was only moderate ($r_s = –0.36$) [51]. Moreover, the fast diagnosis kit revealed questionable sensitivity and specificity rates, reaching 61.1% and 58.7%, respectively [51].

Even though ELISA is a time-consuming method, it is still broadly used when laboratory infrastructure is available. However, current data analysis does not consider it to have high potential for point-of-care or calf-side applications.

2.5. Ionization techniques (IT) and mass spectrometry (MS)

IT such as solid or liquid matrix-assisted laser desorption/ionization (MALDI) are considered core techniques for molecular analysis through MS [52].

Solid MALDI MS profiling has been applied in many areas [53]. Thus, these attempts were carried out with variable success rates because of many reasons, including the limited analytical power [53]. Generally, liquid MALDI has additional advantages compared to the solid alternative such as greater sample homogeneity, greater ion beam stability, and lower sample consumption [54]. This kind of advanced diagnosis has been used for the detection of dairy cow mastitis, proving 98.5% accuracy and 100% specificity [53].

Liquid MALDI MS is relatively affordable and highly efficient in terms of operating times as it has been previously shown [55] while dealing with sheep and goat milk protein and lipid profiling. Therefore, the latter study has highlighted a new potential alternative for colostrum discrimination via IgG detection. MALDI MS was compared to the presently employed methods, ELISA and BR, and was deemed globally superior [55].

Even if current literature does not state the use of these techniques for FPT evaluation in calves, it has been previously hypothesized that these advanced methods would be at a higher value in comparison with current alternatives [23]. Thus, research activity concerning these applications should be considered.

2.6. Proteomics

Fluid and tissue sample characterization through proteomic studies have been recently discussed, along with their implications in veterinary practice [56-59].

Numerous proteins have been individualized through proteomics, during colostrum or milk analysis. One group identified 212 compounds, 208 being also quantified [59]. The same study highlighted the link between the decrease in protease inhibitors and the subsequent drop in immunoglobulins, suggesting that certain enzymes may have the ability to protect IgG from proteolytic degradation [59]. Recently, IgG identification was reported in a proteomic study regarding colostrum compounds time-related variability [60]. Thus, using a peptide-centric LC–MS/MS, 212 individual proteic sequences have been isolated, >50 % of the colostrum protein content being represented by IgG [60].

Due to still absent information regarding serum compounds analysis in calves for FPT diagnosis, proteomics is still not established for this purpose. However, the results previously reported, particularly those concerning milk or colostrum examination, provide a foundation for a potential new tool that warrants further investigation.

2.7. Infrared spectroscopy (IS) and transmitted & attenuated infrared spectroscopy (ATR)

By courtesy of modern analytical chemistry, another tool has been proposed for different qualitative and quantitative measurements. IS has proved various applications being able to carry out multianalyte analysis [61, 62]. For IgG levels assessment IS has been trialed in humans [63], equines [64], and bovines [65, 66].

One group tested ATR and IR for the measurement of bovine serum IgG concentration, thus FPT diagnosis [67]. The authors have stated that both methods are suitable for the proposed

applications, based on the sensitivity, specificity, and predictive values obtained. Moreover, the use of different sample types was appraised, with optimal cut-off values leading to high levels of agreement (88.1%) between results derived from testing serum and plasma by transmitted IR spectroscopy [21].

Transferability into field conditions was also scrutinized, and a portable ATR-IR spectrometer rendered suitable for use in alpacas [68]. Furthermore, the other rapid methods described [42] in correlation with the previously sketched portable ATR spectrometers [61, 62] have suggested their potential for calf-side applications.

2.8. Electrophoresis and capillary electrophoresis (CE)

Electrophoretic methods can be used to measure immunoglobulin concentrations in serum thanks to the final fraction migration [69]. The latter statement refers to IgG which is the least negatively charged molecule that will determine a slow migration through the electric field [23]. Therefore, it is considered that IgG electrophoretic analysis can be carried out with higher accuracy (89%) [29]. Moreover, a study regarding serum protein profiling has highlighted the utility of electrophoretic findings in general practice situations such as neonatal calf diarrhea [70]. Nevertheless, the studies on ruminants have identified variables that could have affected the outcomes, including the animal's age and physiological condition as well as sample pre-analytical preparations in the lab [71-73].

For FPT assessment in calves, electrophoretic techniques have been applied and current data suggests adequate accuracy when compared to the gold standard (RID) [74].

Electrophoresis was successfully applied for IgG level determination in serum samples after colostrum supplementation in calves [75]. More data is available in equines, and a good agreement between RID and electrophoresis when determining IgG levels in foals being highlighted [76, 77].

Thus, laboratory-based, electrophoresis is an interesting alternative to RID being a faster method, which still relies on specific cut-off values [32].

CE is a superior technique that has been used in human medicine for serum protein recognition [78, 79]. Additionally, CE is more suitable for monoclonal components detection clinical implications of these features being already depicted in related scientific works [79].

Fully automated [79] and cost-efficient [80], CE has been also used for veterinary research purposes regarding FPT. The method was applied in lambs, being considered reliable for serum IgG determination, due to its accordance with the gold standard RID [81]. CE was applied to samples from 216 clinically healthy Holstein Friesian calves, the results proving the high reliability of the method for FPT diagnosis when a cut-off value of 6.9 mg IgG/mL is considered [32].

3. Conclusions

The heightened awareness of a significantly high prevalence of FPT in neonatal calves accentuates the imperative for reliable diagnostic methodologies. This underscores the need for accurate FPT assessment, given the economic implications and increased disease susceptibility that further emphasize the urgency of precise diagnostic tools. While RID serves as the established gold standard, persistent practical limitations necessitate the exploration of alternative approaches. Emerging technologies like immunoturbidimetry, and innovative methodologies such as the STIGA, MS,

and proteomics show promise but require thorough validation for the establishment of practical, efficient modalities to ensure optimal calf health and productivity.

Author Contributions: writing—original draft preparation, D.P., F.P.P., N.T.C, C.R.A.; writing—review and editing, D.P., F.P.P., N.T.C, F.M.; supervision, M.D.C.; All authors have read and agreed to the published version of the manuscript.

Funding: This research received no external funding.

Conflicts of Interest: The authors declare no conflict of interest.

References

1. Borghesi, J.; Mario, L. C.; Rodrigues, M. N.; Favaron, P. O.; Miglino, M. A. Immunoglobulin Transport during Gestation in Domestic Animals and Humans—A Review. *Open J Anim Sci* **2014**, *04* (05), 323–336. https://doi.org/10.4236/ojas.2014.45041.
2. Bragg, R.; Macrae, A.; Lycett, S.; Burrough, E.; Russell, G.; Corbishley, A. Prevalence and Risk Factors Associated with Failure of Transfer of Passive Immunity in Spring Born Beef Suckler Calves in Great Britain. *Prev Vet Med* **2020**, *181*, 105059. https://doi.org/10.1016/j.prevetmed.2020.105059.
3. Constantin, N. T.; Sipos, A. Passive Transfer of Immunoglobulins from Ewe to Lamb. *Scientific Works. Series C* **2021**, *LXVII* (1), 53–58. https://veterinarymedicinejournal.usamv.ro/index.php/scientific-papers/past-issues?id=1723
4. Geiger, A. J. Colostrum: Back to Basics with Immunoglobulins. *J Anim Sci* **2020**, *98* (Supplement_1), S126–S132. https://doi.org/10.1093/jas/skaa142.
5. Bessi, R.; Pauletti, P.; d'Arce, R. D.; Machado Neto, R. Absorção de Anticorpos Do Colostro Em Bezerros: I. Estudo No Intestino Delgado Proximal. *Revista Brasileira de Zootecnia* **2002**, *31* (6), 2314–2324. https://doi.org/10.1590/S1516-35982002000900021.
6. Godden, S. Colostrum Management for Dairy Calves. *Veterinary Clinics of North America: Food Animal Practice* **2008**, *24* (1), 19–39. https://doi.org/10.1016/j.cvfa.2007.10.005.
7. Raboisson, D.; Trillat, P.; Cahuzac, C. Failure of Passive Immune Transfer in Calves: A Meta-Analysis on the Consequences and Assessment of the Economic Impact. *PLoS One* **2016**, *11* (3), e0150452. https://doi.org/10.1371/journal.pone.0150452.
8. Mee, J. Why Do So Many Calves Die on Modern Dairy Farms and What Can We Do about Calf Welfare in the Future? *Animals* **2013**, *3* (4), 1036–1057. https://doi.org/10.3390/ani3041036.
9. Lichtmannsperger, K.; Hartsleben, C.; Spöcker, M.; Hechenberger, N.; Tichy, A.; Wittek, T. Factors Associated with Colostrum Quality, the Failure of Transfer of Passive Immunity, and the Impact on Calf Health in the First Three Weeks of Life. *Animals* **2023**, *13* (11), 1740. https://doi.org/10.3390/ani13111740.
10. Pithua, P.; Aly, S. S. *Respiratory Disease in Dairy Calves View Project Stable Flies and Cattle Bunching Behavior View Project*; 2013; Vol. 11. https://www.researchgate.net/publication/235900544.
11. Donovan, G. A.; Dohoo, I. R.; Montgomery, D. M.; Bennett, F. L. Associations between Passive Immunity and Morbidity and Mortality in Dairy Heifers in Florida, USA. *Prev Vet Med* **1998**, *34* (1), 31–46. https://doi.org/10.1016/S0167-5877(97)00060-3.
12. Atkinson, D. J.; von Keyserlingk, M. A. G.; Weary, D. M. Benchmarking Passive Transfer of Immunity and Growth in Dairy Calves. *J Dairy Sci* **2017**, *100* (5), 3773–3782. https://doi.org/10.3168/jds.2016-11800.
13. Calloway, C. D.; Tyler, J. W.; Tessman, R. K.; Hostetler, D.; Holle, J. Comparison of Refractometers and Test Endpoints in the Measurement of Serum Protein Concentration to Assess Passive Transfer Status in Calves. *J Am Vet Med Assoc* **2002**, *221* (11), 1605–1608. https://doi.org/10.2460/javma.2002.221.1605.
14. Waldner, C. L.; Rosengren, L. B. Factors Associated with Serum Immunoglobulin Levels in Beef Calves from Alberta and Saskatchewan and Association between Passive Transfer and Health Outcomes. *Can Vet J* **2009**, *50* (3), 275–281.

15. Dewell, R. D.; Hungerford, L. L.; Keen, J. E.; Laegreid, W. W.; Griffin, D. D.; Rupp, G. P.; Grotelueschen, D. M. Association of Neonatal Serum Immunoglobulin G1 Concentration with Health and Performance in Beef Calves. *J Am Vet Med Assoc* **2006**, *228* (6), 914–921. https://doi.org/10.2460/javma.228.6.914.
16. Roadknight, N.; Jongman, E.; Mansell, P.; Courtman, N.; McGill, D.; Hepworth, G.; Fisher, A. Prevalence of Failure of Passive Immunity Transfer in Australian Non-Replacement Dairy Calves. *Aust Vet J* **2022**, *100* (7), 292–295. https://doi.org/10.1111/avj.13160.
17. Bresciani, C.; Sabbioni, A.; Ciampoli, R.; Bertocchi, M.; Saleri, R.; Cabassi, C. S.; Bigliardi, E.; Di Ianni, F.; Parmigiani, E. An Innovative Hyperimmune Bovine Plasma for Prophylaxis and Therapy of Neonatal Dairy Calf Diarrhea-a Clinical Trial. *Large Animal Review* **2016**, *22*, 115–119.
18. Constantin, N. T.; Posastiuc, F. P.; Andrei, C. R.; Sprințu, I. C.; Ionescu, T. Ștefan; Bărăităreanu, S. Blood Processing in Cattle: Insights for Alternative Therapies. *Rev Rom Med Vet* **2023**, *33* (3), 46–50.
19. Urie, N. J.; Lombard, J. E.; Shivley, C. B.; Kopral, C. A.; Adams, A. E.; Earleywine, T. J.; Olson, J. D.; Garry, F. B. Preweaned Heifer Management on US Dairy Operations: Part I. Descriptive Characteristics of Preweaned Heifer Raising Practices. *J Dairy Sci* **2018**, *101* (10), 9168–9184. https://doi.org/10.3168/jds.2017-14010.
20. Cuttance, E.; Mason, W.; Laven, R.; McDermott, J.; Phyn, C. Prevalence and Calf-Level Risk Factors for Failure of Passive Transfer in Dairy Calves in New Zealand. *N Z Vet J* **2017**, *65* (6), 297–304. https://doi.org/10.1080/00480169.2017.1361876.
21. Elsohaby, I.; McClure, J. T.; Waite, L. A.; Cameron, M.; Heider, L. C.; Keefe, G. P. Using Serum and Plasma Samples to Assess Failure of Transfer of Passive Immunity in Dairy Calves. *J Dairy Sci* **2019**, *102* (1), 567–577. https://doi.org/10.3168/jds.2018-15070.
22. Constantin, N. T.; Posastiuc, F. P.; Andrei, C. R.; Sprințu, I. C.; Bărăităreanu, S. Indirect Passive Transfer Evaluation Techniques in Calves: A Review. *Rev Rom Med Vet* **2023**, *33* (4), 97–101.
23. de Souza, R. S.; dos Santos, L. B. C.; Melo, I. O.; Cerqueira, D. M.; Dumas, J. V.; Leme, F. de O. P.; Moreira, T. F.; Meneses, R. M.; de Carvalho, A. U.; Facury-Filho, E. J. Current Diagnostic Methods for Assessing Transfer of Passive Immunity in Calves and Possible Improvements: A Literature Review. *Animals* **2021**, *11* (10), 2963. https://doi.org/10.3390/ani11102963.
24. Elsohaby, I.; McClure, J. T.; Keefe, G. P. Evaluation of Digital and Optical Refractometers for Assessing Failure of Transfer of Passive Immunity in Dairy Calves. *J Vet Intern Med* **2015**, *29* (2), 721–726. https://doi.org/10.1111/jvim.12560.
25. Bielmann, V.; Gillan, J.; Perkins, N. R.; Skidmore, A. L.; Godden, S.; Leslie, K. E. An Evaluation of Brix Refractometry Instruments for Measurement of Colostrum Quality in Dairy Cattle. *J Dairy Sci* **2010**, *93* (8), 3713–3721. https://doi.org/10.3168/jds.2009-2943.
26. Davis, R.; Giguère, S. Evaluation of Five Commercially Available Assays and Measurement of Serum Total Protein Concentration via Refractometry for the Diagnosis of Failure of Passive Transfer of Immunity in Foals. *J Am Vet Med Assoc* **2005**, *227* (10), 1640–1645. https://doi.org/10.2460/javma.2005.227.1640.
27. Drikic, M.; Windeyer, C.; Olsen, S.; Fu, Y.; Doepel, L.; De Buck, J. Determining the IgG Concentrations in Bovine Colostrum and Calf Sera with a Novel Enzymatic Assay. *J Anim Sci Biotechnol* **2018**, *9* (1), 69. https://doi.org/10.1186/s40104-018-0287-4.
28. Mancini, G.; Carbonara, A. O.; Heremans, J. F. Immunochemical Quantitation of Antigens by Single Radial Immunodiffusion. *Immunochemistry* **1965**, *2* (3), 235-IN6. https://doi.org/10.1016/0019-2791(65)90004-2.
29. Pfeiffer, N. E.; McGuire, T. C.; Bendel, R. B.; Weikel, J. M. Quantitation of Bovine Immunoglobulins: Comparison of Single Radial Immunodiffusion, Zinc Sulfate Turbidity, Serum Electrophoresis, and Refractometer Methods. *Am J Vet Res* **1977**, *38* (5), 693–698.
30. Penhale, W. J.; Christie, G. Quantitative Studies on Bovine Immunoglobulins. *Res Vet Sci* **1969**, *10* (6), 493–502. https://doi.org/10.1016/S0034-5288(18)34382-0.

31. Dunn, A.; Duffy, C.; Gordon, A.; Morrison, S.; Argűello, A.; Welsh, M.; Earley, B. Comparison of Single Radial Immunodiffusion and ELISA for the Quantification of Immunoglobulin G in Bovine Colostrum, Milk and Calf Sera. *J Appl Anim Res* **2018**, *46* (1), 758–765. https://doi.org/10.1080/09712119.2017.1394860.
32. Sutter, F.; Rauch, E.; Erhard, M.; Sargent, R.; Weber, C.; Heuwieser, W.; Borchardt, S. Evaluation of Different Analytical Methods to Assess Failure of Passive Transfer in Neonatal Calves. *J Dairy Sci* **2020**, *103* (6), 5387–5397. https://doi.org/10.3168/jds.2019-17928.
33. Gelsinger, S. L.; Smith, A. M.; Jones, C. M.; Heinrichs, A. J. Technical Note: Comparison of Radial Immunodiffusion and ELISA for Quantification of Bovine Immunoglobulin G in Colostrum and Plasma. *J Dairy Sci* **2015**, *98* (6), 4084–4089. https://doi.org/10.3168/jds.2014-8491.
34. Akköse, M.; Karabulut, E.; Yılmaz, İ. Ç.; Dik, Ç.; İnal, Ş.; Özbeyaz, C.; Çam, M.; Çınar, E. M.; Orakçı, D.; Durmaz, M. Evaluation of Refractometry Methods for Estimating Passive Immunity Status in Neonatal Foals. *J Immunol Methods* **2022**, *510*, 113359. https://doi.org/10.1016/j.jim.2022.113359.
35. Ameri, M.; Wilkerson, M. J. Comparison of Two Commercial Radial Immunodiffusion Assays for Detection of Bovine Immunoglobulin G in Newborn Calves. *Journal of Veterinary Diagnostic Investigation* **2008**, *20* (3), 333–336. https://doi.org/10.1177/104063870802000312.
36. Bassols, A.; Robles-Guirado, J. A.; Arroyo, L.; Soler, L.; García, N.; Pato, R.; Peña, R.; Saco, Y.; Armengol, R.; Lampreave, F.; Alava, M. A.; Canalias, F.; Piñeiro, M. Validation of New Automated Turbidimetric Immunoassays for the Measurement of Haptoglobin and Inter-α-trypsin Inhibitor Heavy Chain <scp>H4</Scp> Specific for the Bovine Species. *Vet Clin Pathol* **2023**, *52* (S1), 64–74. https://doi.org/10.1111/vcp.13164.
37. Alley, M. L.; Haines, D. M.; Smith, G. W. Evaluation of Serum Immunoglobulin G Concentrations in Dairy Calves by Use of an Automated Turbidimetric Immunoassay. *American Association of Bovine Practitioners Conference Proceedings* **2012**, 230. https://doi.org/10.21423/aabppro20123939.
38. Etzel, L. *Development of an Automated Turbidimetric Immunoassay for Quantification of Bovine Serum Immunoglobulin G Antigen Purification View Project*; 1997. https://www.researchgate.net/publication/13867742.
39. Ujvari, S.; Schwarzwald, C. C.; Fouché, N.; Howard, J.; Schoster, A. Validation of a Point-of-Care Quantitative Equine IgG Turbidimetric Immunoassay and Comparison of IgG Concentrations Measured with Radial Immunodiffusion and a Point-of-Care IgG ELISA. *J Vet Intern Med* **2017**, *31* (4), 1170–1177. https://doi.org/10.1111/jvim.14770.
40. Kreuder, A. J.; Breuer, R. M.; Wiley, C.; Dohlman, T.; Smith, J. S.; McKeen, L. Comparison of Turbidometric Immunoassay, Refractometry, and Gamma-glutamyl Transferase to Radial Immunodiffusion for Assessment of Transfer of Passive Immunity in High-risk Beef Calves. *J Vet Intern Med* **2023**. https://doi.org/10.1111/jvim.16831.
41. Renaud, D. L.; Duffield, T. F.; LeBlanc, S. J.; Kelton, D. F. Short Communication: Validation of Methods for Practically Evaluating Failed Passive Transfer of Immunity in Calves Arriving at a Veal Facility. *J Dairy Sci* **2018**, *101* (10), 9516–9520. https://doi.org/10.3168/jds.2018-14723.
42. Elsohaby, I.; Keefe, G. P. Preliminary Validation of a Calf-Side Test for Diagnosis of Failure of Transfer of Passive Immunity in Dairy Calves. *J Dairy Sci* **2015**, *98* (7), 4754–4761. https://doi.org/10.3168/jds.2014-9027.
43. Drikic, M.; De Buck, J. Split Trehalase as a Versatile Reporter for a Wide Range of Biological Analytes. *Biotechnol Bioeng* **2018**, *115* (5), 1128–1136. https://doi.org/10.1002/bit.26556.
44. Drikic, M.; Olsen, S.; De Buck, J. Detecting Total Immunoglobulins in Diverse Animal Species with a Novel Split Enzymatic Assay. *BMC Vet Res* **2019**, *15* (1), 374. https://doi.org/10.1186/s12917-019-2126-z.
45. Chelack, B. J.; Morley, P. S.; Haines, D. M. Evaluation of Methods for Dehydration of Bovine Colostrum for Total Replacement of Normal Colostrum in Calves. *Can Vet J* **1993**, *34* (7), 407–412.

46. Gelsinger, S. L.; Jones, C. M.; Heinrichs, A. J. Effect of Colostrum Heat Treatment and Bacterial Population on Immunoglobulin G Absorption and Health of Neonatal Calves. *J Dairy Sci* **2015**, *98* (7), 4640–4645. https://doi.org/10.3168/jds.2014-8790.
47. Baumrucker, C. R.; Bruckmaier, R. M. Colostrogenesis: IgG1 Transcytosis Mechanisms. *J Mammary Gland Biol Neoplasia* **2014**, *19* (1), 103–117. https://doi.org/10.1007/s10911-013-9313-5.
48. Vetter, A.; Argüello, A.; Baumrucker, C.; Bruckmaier, R. M. Short Communication: Fractional Milking Distribution of Immunoglobulin G and Other Constituents in Colostrum. *J Dairy Sci* **2013**, *96* (9), 5919–5922. https://doi.org/10.3168/jds.2013-6745.
49. Lee, S.-H.; Jaekal, J.; Bae, C.-S.; Chung, B.-H.; Yun, S.-C.; Gwak, M.-J.; Noh, G.-J.; Lee, D.-H. Enzyme-Linked Immunosorbent Assay, Single Radial Immunodiffusion, and Indirect Methods for the Detection of Failure of Transfer of Passive Immunity in Dairy Calves. *J Vet Intern Med* **2008**, *22* (1), 212–218. https://doi.org/10.1111/j.1939-1676.2007.0013.x.
50. Quigley, J. D.; Lago, A.; Chapman, C.; Erickson, P.; Polo, J. Evaluation of the Brix Refractometer to Estimate Immunoglobulin G Concentration in Bovine Colostrum. *J Dairy Sci* **2013**, *96* (2), 1148–1155. https://doi.org/10.3168/jds.2012-5823.
51. Hampe, M.; Söllner-Donat, S.; Failing, K.; Wehrend, A. Comparison of Enzyme-Linked Immunosorbent Assay and Fassisi® Bovine Immunoglobulin G (IgG) Immunoassay for Quantification of Bovine IgG in Neonatal Calf Serum. *Vet World* **2021**, 3211–3215. https://doi.org/10.14202/vetworld.2021.3211-3215.
52. Ryumin, P.; Brown, J.; Morris, M.; Cramer, R. Investigation and Optimization of Parameters Affecting the Multiply Charged Ion Yield in AP-MALDI MS. *Methods* **2016**, *104*, 11–20. https://doi.org/10.1016/j.ymeth.2016.01.015.
53. Hale, O. J.; Morris, M.; Jones, B.; Reynolds, C. K.; Cramer, R. Liquid Atmospheric Pressure Matrix-Assisted Laser Desorption/Ionization Mass Spectrometry Adds Enhanced Functionalities to MALDI MS Profiling for Disease Diagnostics. *ACS Omega* **2019**, *4* (7), 12759–12765. https://doi.org/10.1021/acsomega.9b01476.
54. Ryumin, P.; Brown, J.; Morris, M.; Cramer, R. Protein Identification Using a NanoUHPLC-AP-MALDI MS/MS Workflow with CID of Multiply Charged Proteolytic Peptides. *Int J Mass Spectrom* **2017**, *416*, 20–28. https://doi.org/10.1016/j.ijms.2016.12.006.
55. Piras, C.; Ceniti, C.; Hartmane, E.; Costanzo, N.; Morittu, V. M.; Roncada, P.; Britti, D.; Cramer, R. Rapid Liquid AP-MALDI MS Profiling of Lipids and Proteins from Goat and Sheep Milk for Speciation and Colostrum Analysis. *Proteomes* **2020**, *8* (3), 20. https://doi.org/10.3390/proteomes8030020.
56. Yilmaz, Z.; Eralp Inan, O.; Kocaturk, M.; Baykal, A. T.; Hacariz, O.; Hatipoglu, I.; Tvarijonaviciute, A.; Cansev, M.; Ceron, J.; Ulus, I. H. Changes in Serum Proteins after Endotoxin Administration in Healthy and Choline-Treated Calves. *BMC Vet Res* **2016**, *12* (1), 210. https://doi.org/10.1186/s12917-016-0837-y.
57. Kacar, Y.; Baykal, A. T.; Aydin, L.; Batmaz, H. Evaluation of the Efficacy of Cow Colostrum in the Treatment and Its Effect on Serum Proteomes in Calves with Cryptosporidiosis. *Vet Immunol Immunopathol* **2022**, *248*, 110429. https://doi.org/10.1016/j.vetimm.2022.110429.
58. Mann, S.; Curone, G.; Chandler, T. L.; Sipka, A.; Cha, J.; Bhawal, R.; Zhang, S. Heat Treatment of Bovine Colostrum: II. Effects on Calf Serum Immunoglobulin, Insulin, and IGF-I Concentrations, and the Serum Proteome. *J Dairy Sci* **2020**, *103* (10), 9384–9406. https://doi.org/10.3168/jds.2020-18619.
59. Zhang, L.; Boeren, S.; Hageman, J. A.; van Hooijdonk, T.; Vervoort, J.; Hettinga, K. Bovine Milk Proteome in the First 9 Days: Protein Interactions in Maturation of the Immune and Digestive System of the Newborn. *PLoS One* **2015**, *10* (2), e0116710. https://doi.org/10.1371/journal.pone.0116710.
60. Gazi, I.; Reiding, K. R.; Groeneveld, A.; Bastiaans, J.; Huppertz, T.; Heck, A. J. R. Key Changes in Bovine Milk Immunoglobulin G during Lactation: NeuAc Sialylation Is a Hallmark of Colostrum Immunoglobulin G *N* -Glycosylation. *Glycobiology* **2023**, *33* (2), 115–125. https://doi.org/10.1093/glycob/cwad001.
61. Da-Wen Sun. *Infrared Spectroscopy for Food Quality Analysis and Control*, 1st ed.; London: Academic, 2009.

62. Smith B.C: *Fundamentals of Fourier Transform Infrared Spectroscopy*, 2nd ed.; CRC Press: Boca Raton, USA, 2011.
63. Hou, S.; McClure, J. T.; Shaw, R. A.; Riley, C. B. Immunoglobulin G Measurement in Blood Plasma Using Infrared Spectroscopy. *Appl Spectrosc* **2014**, *68* (4), 466–474. https://doi.org/10.1366/12-06869.
64. Riley, C. B.; McClure, J. T.; Low-Ying, S.; Shaw, R. A. Use of Fourier-Transform Infrared Spectroscopy for the Diagnosis of Failure of Transfer of Passive Immunity and Measurement of Immunoglobulin Concentrations in Horses. *J Vet Intern Med* **2007**, *21* (4), 828–834. https://doi.org/10.1892/0891-6640(2007)21[828:uofisf]2.0.co;2.
65. Goi, A.; Costa, A.; Visentin, G.; De Marchi, M. Mid-Infrared Spectroscopy for Large-Scale Phenotyping of Bovine Colostrum Gross Composition and Immunoglobulin Concentration. *J Dairy Sci* **2023**, *106* (9), 6388–6401. https://doi.org/10.3168/jds.2022-23059.
66. Franzoi, M.; Costa, A.; Goi, A.; Penasa, M.; De Marchi, M. Effectiveness of Visible – Near Infrared Spectroscopy Coupled with Simulated Annealing Partial Least Squares Analysis to Predict Immunoglobulins G, A, and M Concentration in Bovine Colostrum. *Food Chem* **2022**, *371*, 131189. https://doi.org/10.1016/j.foodchem.2021.131189.
67. Elsohaby, I.; McClure, J. T.; Riley, C. B.; Shaw, R. A.; Keefe, G. P. Quantification of Bovine Immunoglobulin G Using Transmission and Attenuated Total Reflectance Infrared Spectroscopy. *Journal of Veterinary Diagnostic Investigation* **2016**, *28* (1), 30–37. https://doi.org/10.1177/1040638715613101.
68. Elsohaby, I.; Burns, J. B.; Riley, C. B.; Shaw, R. A.; McClure, J. T. Application of Laboratory and Portable Attenuated Total Reflectance Infrared Spectroscopic Approaches for Rapid Quantification of Alpaca Serum Immunoglobulin G. *PLoS One* **2017**, *12* (6), e0179644. https://doi.org/10.1371/journal.pone.0179644.
69. Marc, S.; Kirovski, D.; Mircu, C.; Hutu, I.; Otavă, G.; Paul, C.; Boldura, O.; Tulcan, C. Serum Protein Electrophoretic Pattern in Neonatal Calves Treated with Clinoptilolite. *Molecules* **2018**, *23* (6), 1278. https://doi.org/10.3390/molecules23061278.
70. Choi, K.-S.; Kang, J.-H.; Cho, H.-C.; Yu, D.-H.; Park, J. Changes in Serum Protein Electrophoresis Profiles and Acute Phase Proteins in Calves with Diarrhea. *Can J Vet Res* **2021**, *85* (1), 45–50.
71. Piccione, G.; Alberghina, D.; Marafioti, S.; Giannetto, C.; Casella, S.; Assenza, A.; Fazio, F. Electrophoretic Serum Protein Fraction Profile During the Different Physiological Phases in Comisana Ewes. *Reproduction in Domestic Animals* **2012**, *47* (4), 591–595. https://doi.org/10.1111/j.1439-0531.2011.01925.x.
72. Tóthová, C.; Nagy, O.; Seidel, H.; Kováč, G. Serum Protein Electrophoretic Pattern in Clinically Healthy Calves and Cows Determined by Agarose Gel Electrophoresis. *Comp Clin Path* **2013**, *22* (1), 15–20. https://doi.org/10.1007/s00580-011-1363-8.
73. Piccione, G.; Casella, S.; Giannetto, C.; Panzera, M.; Pennisi, P.; Alberghina, D. Influence of Short-Term Storage on Electrophoretic Profile of Bovine Serum Proteins. *J Appl Anim Res* **2014**, *42* (1), 123–125. https://doi.org/10.1080/09712119.2013.795900.
74. Massimini, G.; Peli, A.; Boari, A.; Britti, D. Evaluation of Assay Procedures for Prediction of Passive Transfer Status in Lambs. *Am J Vet Res* **2006**, *67* (4), 593–598. https://doi.org/10.2460/ajvr.67.4.593.
75. Lora, I.; Gottardo, F.; Bonfanti, L.; Stefani, A. L.; Soranzo, E.; Dall'Ava, B.; Capello, K.; Martini, M.; Barberio, A. Transfer of Passive Immunity in Dairy Calves: The Effectiveness of Providing a Supplementary Colostrum Meal in Addition to Nursing from the Dam. *Animal* **2019**, *13* (11), 2621–2629. https://doi.org/10.1017/S1751731119000879.
76. Turini, L.; Bonelli, F.; Nocera, I.; Meucci, V.; Conte, G.; Sgorbini, M. Evaluation of Different Methods to Estimate the Transfer of Immunity in Donkey Foals Fed with Colostrum of Good IgG Quality: A Preliminary Study. *Animals* **2021**, *11* (2), 507. https://doi.org/10.3390/ani11020507.
77. Tscheschlok, L.; Venner, M.; Howard, J. Comparison of IgG Concentrations by Radial Immunodiffusion, Electrophoretic Gamma Globulin Concentrations and Total Globulins in Neonatal Foals. *Equine Vet J* **2017**, *49* (2), 149–154. https://doi.org/10.1111/evj.12575.

78. Crivellente, F.; Bonato, M.; Cristofori, P. Analysis of Mouse, Rat, Dog, Marmoset, and Human Serum Proteins by Capillary Electrophoresis: Comparison with Agarose Gel Electrophoresis. *Vet Clin Pathol* **2008**, *37* (1), 73–78. https://doi.org/10.1111/j.1939-165X.2008.00008.x.
79. Regeniter, A.; Siede, W. H. Peaks and Tails: Evaluation of Irregularities in Capillary Serum Protein Electrophoresis. *Clin Biochem* **2018**, *51*, 48–55. https://doi.org/10.1016/j.clinbiochem.2017.09.017.
80. Petersen, J. R.; Okorodudu, A. O.; Mohammad, A.; Payne, D. A. Capillary Electrophoresis and Its Application in the Clinical Laboratory. *Clinica Chimica Acta* **2003**, *330* (1–2), 1–30. https://doi.org/10.1016/S0009-8981(03)00006-8.
81. Morittu, V. M.; Lopreiato, V.; Ceniti, C.; Spina, A. A.; Minuti, A.; Trevisi, E.; Britti, D.; Trimboli, F. Technical Note: Capillary Electrophoresis as a Rapid Test for the Quantification of Immunoglobulin G in Serum of Newborn Lambs. *J Dairy Sci* **2020**, *103* (7), 6583–6587. https://doi.org/10.3168/jds.2019-17859.